European Journal of Radiology Open 8 (2021) 100324

Contents lists available at ScienceDirect

European Journal of Radiology Open

journal homepage: www.elsevier.com/locate/ejro

# Dual energy imaging in cardiothoracic pathologies: A primer for radiologists and clinicians

Amit Gupta [a,*], Elias G Kikano [a], Kaustav Bera [b], Dhiraj Baruah [c], Sachin S Saboo [d], Simon Lennartz [e], Nils Große Hokamp [e], Ali Gholamrezanezhad [f], Robert C Gilkeson [a], Kai R Laukamp [e]

[a] Department of Radiology, University Hospitals Cleveland Medical Center/Case Western Reserve University, 11100 Euclid Ave, Cleveland, OH, 44106, USA
[b] Department of Biomedical Engineering, Case Western Reserve University, Cleveland, OH, USA
[c] Department of Radiology, Medical University of South Carolina, Charleston, SC, USA
[d] Department of Radiology, University Of Texas Health Science Center, San Antonio, TX, USA
[e] Institute for Diagnostic and Interventional Radiology, University Hospital Cologne, Cologne, Germany
[f] Department of Radiology, Keck School of Medicine, University of Southern California, Los Angeles, CA, USA

ARTICLE INFO

*Keywords:*
Dual energy CT
Dual energy radiography
Photoelectric effect

ABSTRACT

Recent advances in dual-energy imaging techniques, dual-energy subtraction radiography (DESR) and dual-energy CT (DECT), offer new and useful additional information to conventional imaging, thus improving assessment of cardiothoracic abnormalities. DESR facilitates detection and characterization of pulmonary nodules. Other advantages of DESR include better depiction of pleural, lung parenchymal, airway and chest wall abnormalities, detection of foreign bodies and indwelling devices, improved visualization of cardiac and coronary artery calcifications helping in risk stratification of coronary artery disease, and diagnosing conditions like constrictive pericarditis and valvular stenosis. Commercially available DECT approaches are classified into emission based (dual rotation/spin, dual source, rapid kilovoltage switching and split beam) and detector-based (dual layer) systems. DECT provide several specialized image reconstructions. Virtual non-contrast images (VNC) allow for radiation dose reduction by obviating need for true non contrast images, low energy virtual mono-energetic images (VMI) boost contrast enhancement and help in salvaging otherwise non-diagnostic vascular studies, high energy VMI reduce beam hardening artifacts from metallic hardware or dense contrast material, and iodine density images allow quantitative and qualitative assessment of enhancement/iodine distribution. The large amount of data generated by DECT can affect interpreting physician efficiency but also limit clinical adoption of the technology. Optimization of the existing workflow and streamlining the integration between post-processing software and picture archiving and communication system (PACS) is therefore warranted.

## 1. Introduction

In conventional radiographic and computed tomography (CT) imaging, the materials with different elemental compositions can demonstrate same or very similar attenuation. Therefore, soft tissue contrast is low and differentiating between different tissues is challenging. The emergence of newer dual-energy technology improves upon this limitation by using the differing attenuation characteristics of tissue at two different X-Ray energies. Understanding the basic physics and common dual-energy images/reconstructions is important for radiologist and clinicians alike to increase diagnostic confidence. Large amounts of post-processed data from dual-energy imaging, particularly dual-energy computed tomography (DECT), poses a challenge for image storage; therefore existing workflow and imaging protocols require

*Abbreviations:* DECT, dual-energy computed tomography; DESR, dual-energy subtraction radiography; keV, kilo electron volt; SNR, signal to noise ratio; CAD, computer-aided detection; VMI, virtual mono-energetic images; VNC, virtual non-contrast images; PACS, picture archiving and communication system; TAVI, transcatheter aortic valve implantation; SPECT, single photon emission computed tomography; PET, positron emission tomography; NIH, national institute of health; AI, artificial intelligence; PPV, positive predictive value; NPV, negative predictive value; kV, kilo volt; CR, computed radiography; BT, blalock-taussig; eGFR, estimated glomerular filtration rate; SVC, superior vena cava; TNC, true non contrast; PCD, photon-counting detector.

* Corresponding author.
*E-mail address:* Amit.Gupta@uhhospitals.org (A. Gupta).

https://doi.org/10.1016/j.ejro.2021.100324
Received 7 December 2020; Received in revised form 5 January 2021; Accepted 6 January 2021

**Table 1**
Advantages and disadvantages of commercially available dual energy imaging techniques.

| Technique | Advantage | Disadvantage |
|---|---|---|
| **Dual energy Subtraction Radiography** | | |
| Single exposure | Standard dose of radiation exposure | Utilizes photostimulable phosphor as detector, therefore has relatively lower SNR |
| | Relative lack of motion artefacts | Compromised energy subtraction, limits lesion conspicuity in subtracted image |
| Double exposure | Utilizes direct digital radiography technique/ amorphous silicon-based detector, therefore has relatively higher SNR | Presence of artifacts due to patient motion |
| | Improved image quality | Increased radiation exposure |
| **Dual energy CT** | | |
| Dual Source (Two x-ray tubes and two sets of detectors scanning simultaneously at two different energies) | Tube current and potential can be optimized independently for both tubes, resulting in better dose and noise characteristics. | Small field of view for low energy tube limiting usage in big patients. |
| | Better spectral separation, improving contrast to noise ratio on material specific images | Asynchronous projection of low and high energy data, precludes material decomposition in x ray projection domain<br>Requires specialized scatter correction.<br>Requires prospective protocol selection |
| Rapid kilo voltage switching (Rapid switching of x ray tube potential between low and high energies within a single rotation) | Near simultaneous data acquisitions of low and high energy data allows for material decomposition in x ray projection domain. | Inability to modulate tube current and potential independently for both tubes, resulting in suboptimal dose and noise characteristics.<br>High overlap between energy spectra<br>Requires prospective protocol selection |
| | No field of view restrictions. | Susceptibility to motion misregistration between low and energy scans. |
| | Cost effective | |
| Dual rotation/spin (Temporal sequential scanning of same patient at two different tube potentials) | Tube current and potential can be optimized independently. | Higher radiation exposure. |
| | No cross scatter. | Material decomposition in image domain. |
| | No field of view limitations | Requires prospective protocol selection |
| Split beam (Filter used to split a cone beam into two "half-cone" beams with different spectra) | No field of view limitations | Filters limits x-ray flux and require a more powerful x-ray tube.<br>Suboptimal spectral separation |
| | Better spatial and temporal coherence. | Requires prospective protocol selection |
| Dual layer (Single x ray source with dual layer detector enabling separate registration of low and high energy photons) | Does not require prospective protocol selection; DECT information available for every scan. | Same filtration used for both low and high energy acquisitions. |
| | No field of view limitation<br>Simultaneous data acquisition allowing for material decomposition in projection domain | Relatively high overlap of energy spectra<br>Tube potential choice is limited because of energy partition at the detector level. |

modification to effectively utilize this technology.

This article highlights basic physics behind dual-energy subtraction radiography and DECT, reviews the commercially available techniques for acquiring dual-energy imaging, and discusses common dual-energy reconstructions available with their added value in cardiothoracic pathologies. Emerging and future clinical applications will also be reviewed.

## 2. Basic principles of dual energy imaging

The principle of dual-energy technology was developed in the 1980s to help resolve some of the limitations of inherent single-energy detector systems both in radiography and CT [1,2]. Single-energy systems are unable to reliably discern between materials of similar density [3]. This limitation was partially solved by using iodinated contrast agents for better tissue differentiation. These agents carry an added risk of nephrotoxicity and other adverse reactions. [4,5].

Dual-energy systems attempt to overcome single-energy limitations by using the phenomenon that tissues respond differently at altering X-Ray energy or spectrums. Dual-energy systems can provide distinct images for specific tissue types as well as iodine concentration maps. These result in CT or radiography images with far more quantitative interpretation compared to single-energy HU based images. Due to technical limitations such as more noise, errors in registration, and increased acquisition times, dual-energy technologies did not enter clinical application until the last decade. Due to advancement in technology, at present, these systems offer several advantages in clinical image reading compared to single-energy systems (Table 1) [6].

The concept of dual-energy CT is based on how X-Ray photons interact with matter at clinically used energy levels. The two most important interactions that contribute to X-Ray attenuation in the clinical spectrum are the *Photoelectric effect* and the *Compton Scatter* [7,8]. The Photoelectric effect is dependent on the atomic number of a given material and represents the interaction of incident photon with the inner shell electron, which primarily occurs at lower energy levels. Compton scatter is deflection of photons by outer shell electrons which is influenced mainly by the physical density and contributes more to the overall attenuation in higher energy ranges.

In order for the Photoelectric effect to take place, a minimum amount of energy in the photon is required, which is also the most likely energy for those events to occur. Photons with higher or lower energy would have a lower likelihood to cause photoelectric events. This is referred to as the k-edge, which is the energy needed to eject the most strongly bound innermost electrons (K-shell electron). Soft tissues with dominant elements C, H, O and N have very low K-edges ranging from 0.01 to 0.53 kilo electron volt (keV) and thus attenuate low-energy X-rays. However, k-edges of calcium (4.0) and iodine (33.20) are much higher than soft tissues, thus resulting in different attenuation spectrum, making them distinguishable on dual energy imaging. (Fig. 1). Imaging at low x-ray beam energies comparable to k-edge of iodine markedly increase attenuation and boost contrast enhancement, thus allowing for reduction in contrast dose while maintaining same diagnostic quality.

In DECT, the varying contributions of these two effects at different energy levels are exploited in different applications: the generation of virtual monoenergetic images based on linear blending of high and low energy datasets and the generation of material-specific maps or virtual non-contrast images which relies on material decomposition algorithms [9,10].

## 3. Single exposure versus double exposure dual-energy subtraction radiography (DESR)

There are two methods for acquiring dual-energy X-Ray images, the two most commonly used are double exposure and single exposure-based methods [11,12]. Each technique has its own pros and cons; the dual-exposure method has a fast readout capability and has a high signal

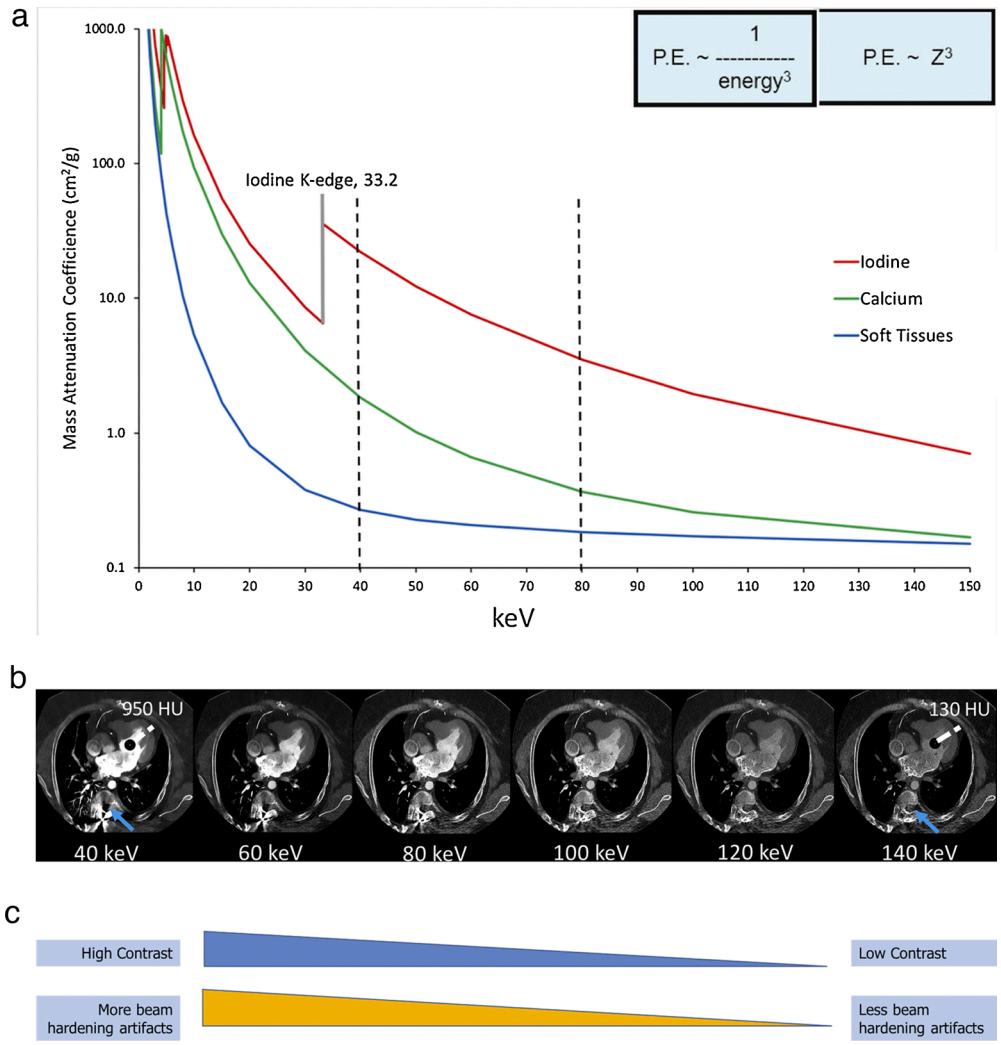


**Fig. 1.** Concept of dual energy imaging. (a) Graph showing dependency of photoelectric effect/attenuation on x ray beam energy and tissue composition/atomic number. The different tissues are better separated on low keV images as compared to high keV images, as annotated by vertical dotted lines. (b and c) Virtual monoenergetic images (VMI) show attenuation comparable to that would be obtained with a true monoenergetic images at specific energy level. Relationship of the image contrast and beam hardening artifacts (Arrows in b) with increasing energy is demonstrated; while image contrast is best at low keV(950 HU at 40 keV versus 130HU at 140 keV in b), beam hardening artifacts are least at higher energies(blue arrows). Note: P.E. = Photoelectric Effect, Z = Atomic number, keV = kilo electron Volt.

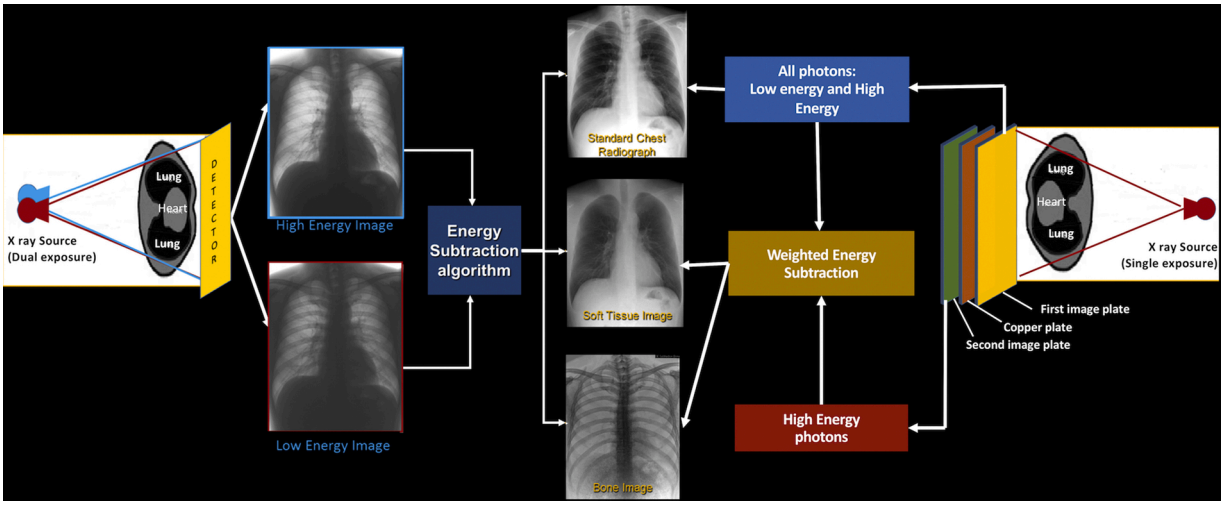


**Fig. 2.** Illustration showing basic principles behind Single exposure and Double exposure Dual-Energy Subtraction Radiography. Double exposure technique requires two exposures to generate high energy and low energy images (typically at 60 kV and 120 kV with 150 ms delay). Subsequent energy subtraction and image post processing yields standard chest radiograph, soft tissue image and bone image. Single exposure technique requires a single x ray exposure. The cassette is composed of a thin copper filter sandwiched between two phosphor computed radiography plates. X-ray beam reaching the first CR plate has both the high and low energy photons, which produces a normal chest radiograph with both bones and soft tissues. The second plate registers the high energy photons only because of intervening first image plate and the filter. After equalization of image contrast and noise characteristics using post processing, weighted subtraction of the images from both layers is performed to generate soft tissue and bone images.

**Table 2**
Clinical applications and benefits of Dual Energy Radiography.

| Clinical application | Type of image (Soft tissue or Bone image) | Added benefit of dual energy radiography |
|---|---|---|
| Lung nodule/ parenchymal abnormality | Soft tissue | Better detection and assessment of blind spots and hidden areas, such as lung apices, retrocardiac lung field and beneath ribs. Improves performance of computer aided detection (CAD) |
| | Bone image | Improved characterization by confirming presence or absence of calcification. |
| Pleural Disease | Soft tissue | Better detection of pleural thickening and pleural based masses. |
| | Bone image | Confirming the calcified pleural plaques in asbestos related pleural disease, reducing need for additional imaging. |
| Mediastinal and hilar lesion | Soft tissue | Improved detection of lymphadenopathy and mediastinal masses. |
| | Bone image | Better visualization of calcifications, important sign of benignity/ granulomatous disease |
| Airways | Soft tissue | Removing overlying bony structures helps in better detection of central airway lesions/masses. Better assessment of airway compromise from masses/ lymphadenopathy and in other situations, such as post intubation, subglottic stenosis in Croup. |
| Pneumothorax | Soft tissue | Increased sensitivity of detection by removing overlying bony structures |
| Vascular disease | Bone image | Improved detection of vascular calcified atherosclerotic disease. Better visualization of myocardial, pericardial and valvular calcifications. |
| Bony lesions | Bone image | Improved detection of benign and malignant osseous lesions and fractures Better differentiation between rib lesions and lung nodules |
| Other incidental findings | Bone image | Improved visualization of radio-opaque foreign bodies, retained post-surgical materials, pacemaker leads, breast implants, catheters and stents |

to noise ratio (SNR) but because of the delay between the two exposures, there is an increase in motion artifacts. Also, due to need for two exposures, this also results in more radiation exposure than single-exposure DESR technique [13,14].The basic principles behind DESR methods and their comparison is highlighted in Fig. 2 and Table 1.

## 4. Clinical utility of DESR

Clinical use of single and dual-exposure subtraction radiography has been studied in evaluating different disease conditions involving different body parts (Table 2). When the dual-energy technique is used in chest radiography, images are displayed in three forms: a regular radiograph without subtraction, a bone selective radiograph, and a soft tissue-selective radiograph.

Overlapping structures like bones can be removed on reconstructed soft issue images. It is possible to enhance visualization of abnormalities in hidden areas compared to conventional radiographs including lung apices, retrocardiac regions, and areas behind bony structures. Low-energy bone images help to improve detection and characterization of bony lesions including primary and secondary neoplasms, fractures, erosions, sclerotic lesions and post-operative changes [13,15,16].

### 4.1. Lung nodule detection

Using the soft tissue-selective DESR image improves identification of lung nodules particularly those obscured by overlapping bone [17]. DESR also increases confidence in identifying the presence or absence of calcification within a lung nodule, an important marker for benignity (Fig. 3) [15]. The addition of computer-aided detection (CAD) with conventional radiograph or dual-energy subtracted soft tissue-selective radiograph has the potential for increasing nodule detection. In one study, Balkman et al. found more nodules combining CAD with dual-energy subtraction radiography when compared to conventional radiography [18]. However, additional studies have failed to show superiority of combining CAD with dual-energy subtraction vs dual-energy subtraction alone. False positive rate of the combined technique in these studies ranged from 1.27 to 5.9 % [19–21].

### 4.2. Lung parenchymal abnormality

The role of DESR is also evaluated in lung parenchymal processes other than nodule detection. In one study, authors found increased sensitivity and interobserver agreement of dual-energy subtracted image over conventional radiographs for the diagnosis of infectious and interstitial lung diseases. There was possible increasing use in patients where detection of parenchymal changes like pneumonia was very important for timely care such as immunocompromised patients [22].

### 4.3. Pleural and mediastinal abnormalities

Dual-energy subtraction radiography may play a role in detecting calcified plaques and identifying patients with asbestos-related pleural plaque disease [15,23]. Soft tissue-selective images from the dual-energy subtraction imaging also helps in improving the ability to identify mediastinal and hilar lesions [24]. Removing the thoracic spine projecting over the airway on frontal radiograph using the dual-energy technique can help visualize tracheal abnormalities including tracheal narrowing and mass effect from adjacent structures [16]. Soft tissue-selective images can also improve the sensitivity of pneumothorax detection (Fig. 4) [25].

### 4.4. Foreign bodies and medical devices

Subtracted images (mostly using the low-energy bone image) is useful in improved visualization of medical support devices and radio-opaque materials, including surgical clips, retained postsurgical materials, breast implants, catheters, stents, and other foreign bodies [13,26,27].

### 4.5. Cardiovascular calcifications

Low-energy bone images from DESR is useful in detecting calcifications, including vascular, valvular, pericardial, myocardial and coronary calcifications. This helps in better detection of coronary artery disease, initiating further workup, and diagnosing conditions such as constrictive pericarditis and valvular stenosis (Fig. 5). Studies have shown improved coronary calcium detection with DESR as compared to plain radiography and sensitivity of DESR ranging from 42 to 52% when compared to CT scanning [28,29]. Mafi et al. in a pilot study evaluated DESR ability to identify high risk patients with coronary artery disease and found excellent correlation between the DESR score and CT coronary calcium score (Correlation coefficient of 0.87), although the accuracy at lower calcium scores was poor. Therefore, refinement and further validation is necessary before DESR can establish itself as an inexpensive and low-radiation imaging tool to risk stratify patients with coronary artery disease. [30].

Aortic valvular calcification is typically present in patients with aortic stenosis and accepted as a marker for severity of aortic stenosis

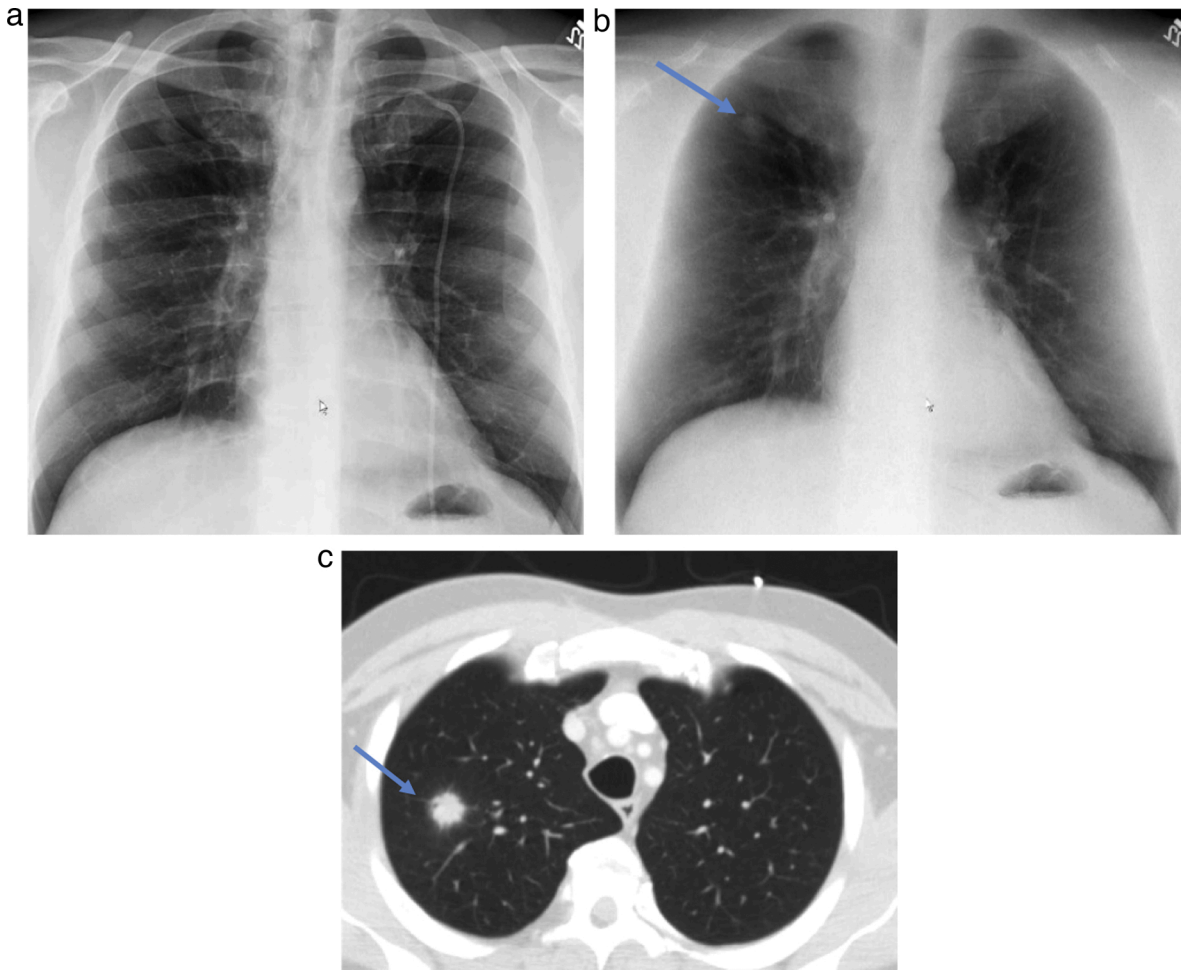


**Fig. 3.** Improved pulmonary nodule detection in a 50-year-old male, s/p stem cell transplant with neutropenia and fever. Conventional radiograph (a) appears unremarkable, but the soft tissue image (b) shows a discrete nodular opacity posterior to the right second rib(Arrow). Subsequent CT scan(c) clearly confirms a solid nodule with subtle ground glass halo(Arrow), which was later proven to be invasive aspergillosis on culture.

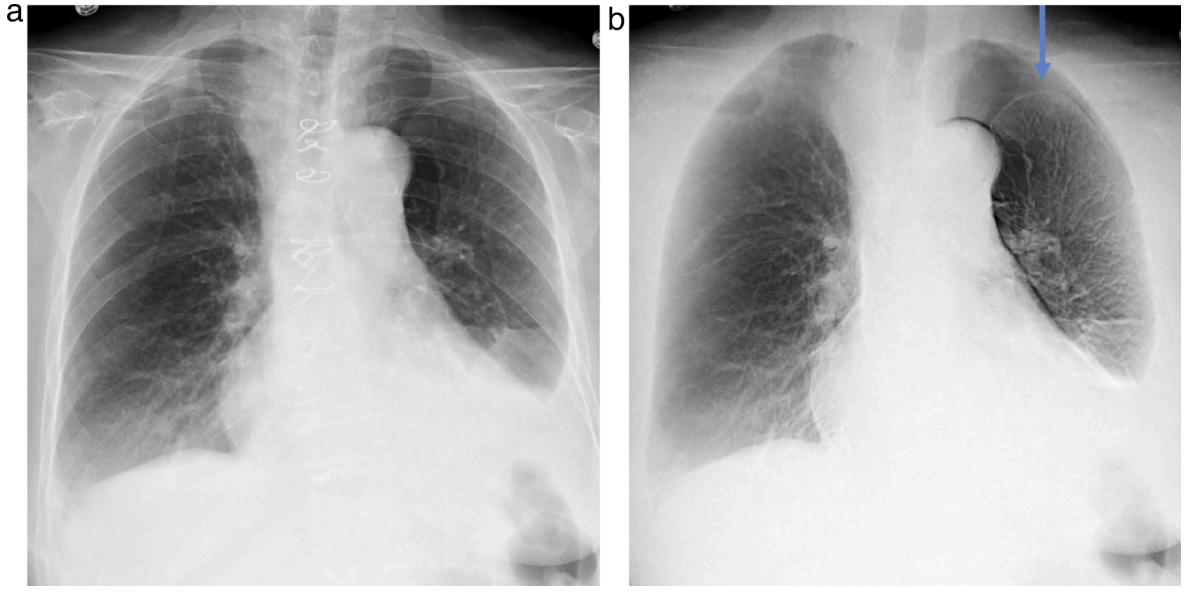


**Fig. 4.** Improved pneumothorax detection in a 45-year-old male following cardiothoracic surgery. Conventional radiograph (a) shows cardiomediastinal silhouette enlargement, mild interstitial pulmonary edema and bilateral pleural effusion. The corresponding soft tissue image (b) shows the hidden left apical pneumothorax (Arrow), which was missed initially on the convention image.

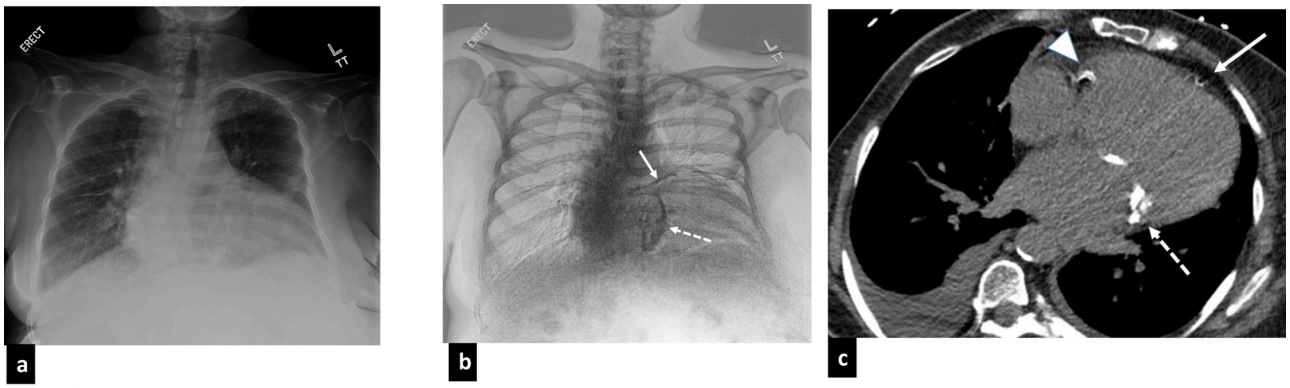


**Fig. 5.** Improved depiction of cardiovascular calcifications in a 70-year-old female with symptoms consistent with congestive heart failure. Conventional X-ray image (a) shows cardiac enlargement with mild vascular congestion and small bilateral pleural effusions in keeping with provided clinical history. Corresponding bone image(b), shows linear calcifications in the expected location of left anterior descending coronary artery (blue arrow) and prominent mitral annular calcification (orange arrow), which were also seen on chest CT (c). Additional right coronary artery calcifications were also seen (white arrow in c), which were likely obscured by scoliotic thoracic spine on radiograph.

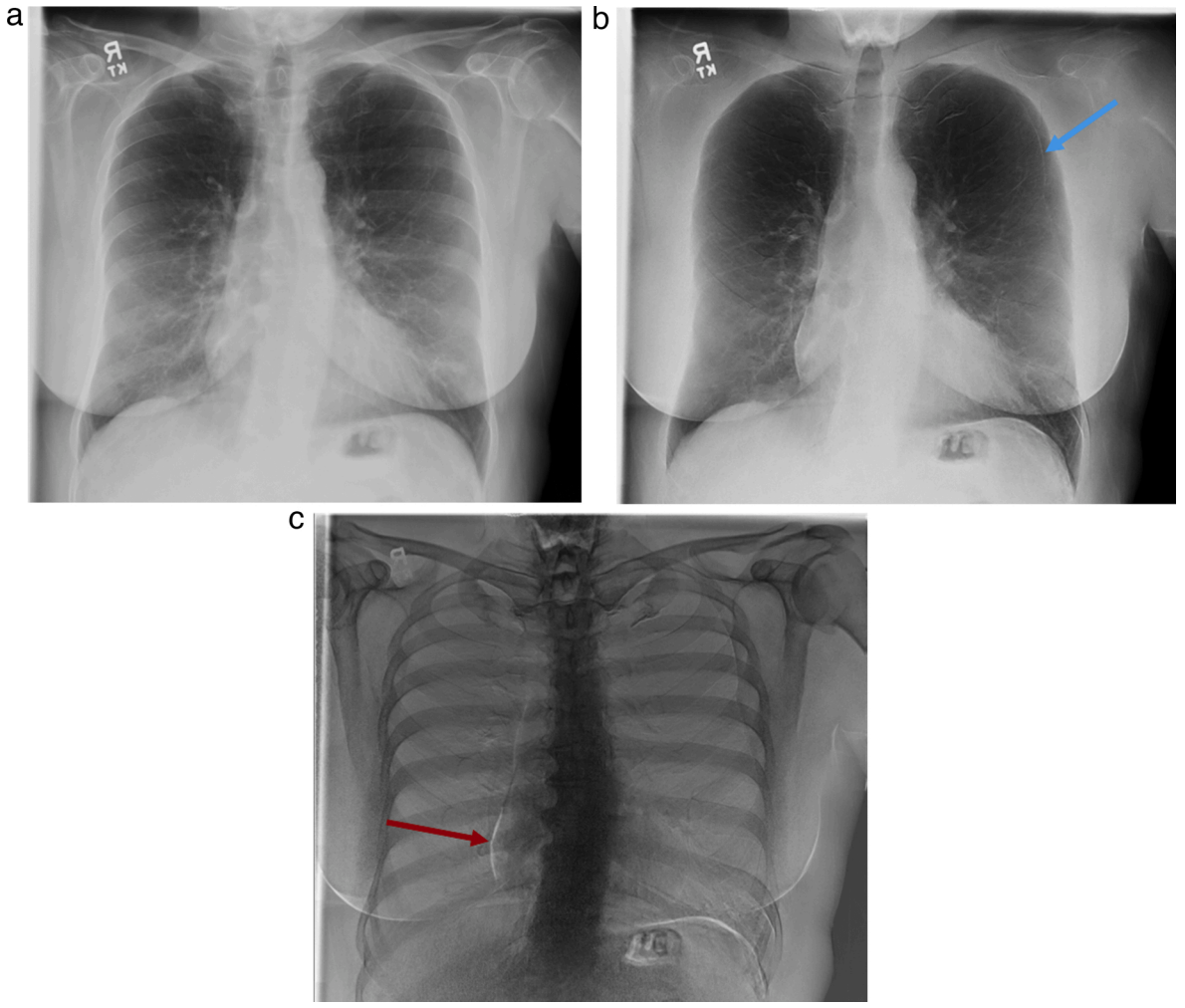


**Fig. 6.** Pitfalls associated with DESR.A 30-year-old male presented with acute onset left side chest pain. The conventional x ray image(a) appears unremarkable, however, on the soft tissue image(b) there is an interface overlying left upper lateral lung, concerning for pneumothorax. Careful correlation with the conventional image reveals it to be an artifact because of incomplete suppression of left scapula (Arrow in b). Also, on bone only image(c) there is a white line along the right heart border which is typical for misregistration artifact from cardiac pulsation (Arrowin c).

[31,32]. There may be some limitation of evaluation of aortic valve calcification in bone selective images as it projects over the spine [33]. Bone selective images are better in depicting mitral annular calcification as the mitral annulus is more laterally positioned as compared to aortic valve (Fig. 5). Bone selective images can help detect subtle pericardial calcification that may be missed on conventional chest radiograph. This

**Table 3**
Dual Energy CT imaging reconstructions and clinical benefits.

| Reconstruction | Method | Benefits |
|---|---|---|
| Virtual Mono-energetic images (VMI) | Obtained by a balanced combination of low and high energy datasets | Low energy VMI<br>Boost of Iodine signal and soft tissue contrast<br>Improvement in Contrast to Noise Ratio.<br>High energy VMI<br>Reduce beam hardening artifact<br>Metal artifact reduction |
| Iodine density | Material density images that allow iodine quantification | Quantification of iodine<br>Eventually helpful for assessment for perfusion, hemodynamic relevance of vessel occlusion, etc |
| Virtual Non Contrast (VNC) | Through identification and removal of iodine | Reduction of radiation since true non contrast phase can be avoided.<br>Helpful in evaluation of incidental findings |
| Z Effective/Overlay image | Computation of color coded images that illustrate the effective atomic number within a voxel. | Color coding is helpful in better lesion delineation.<br>Overlay images also provides additional anatomic information |
| Other reconstructions: | | Limited clinical usage at present time. |
| Non calcium images, | Material decomposition images depicting specific element distribution | Non calcium images helps in reducing blooming artifacts in coronary CT angiogram. |
| Iron maps | | Iron maps have potential to quantify iron deposition in myocardium similar to MRI |

may initiate further work up for constrictive pericarditis in the appropriate clinical setting [33].

### 4.6. Breast imaging

Another potential application of DESR is in the evaluation of breast microcalcifications, an important marker for diagnosing breast cancer. As visualization and detection of microcalcifications is often obscured by superimposed tissues, DESR may help identify microcalcifications by removing overlapping structures. However, it is important to select appropriate imaging parameters when dual-energy subtraction is used for this purpose as the overall noise level will increase [11].

## 5. Pitfalls associated with DESR

### 5.1. Inadequate subtraction

Occasionally, a lung nodule can be detected on the standard image and not displayed on the soft tissue-selective image due to increased noise in the subtracted image [34]. Also, inadequate subtraction of calcified/ossified structures superimposed on a lung nodule can mistakenly identify it as a calcified nodule [15]. Suboptimal suppression of bony structures may also produce artefactual lines and interfaces along the periphery of the lung simulating a pneumothorax (Fig. 6b)

### 5.2. Misregistration

In the dual exposure DESR technique, the delay between the exposures may lead to a misregistration artifact. This is important when there is motion in the imaged volume (i.e. respiration and cardiac contraction) appearing as white or black lines particularly in the bone selective image along with the moving structures (i.e. along with heart, diaphragm, bowel, etc.). This should not be interpreted as an underlying pathology (Fig. 6c).

### 5.3. Radiation exposure

Compared to conventional radiography DESR results in higher radiation doses, with overall increase of radiation dose of up to 16 % as per one study. This warrants judicious use of this technology especially in pediatric patients [22].

## 6. Approaches to dual energy CT and image reconstructions

Early investigations into dual-energy CT (DECT) were published in 1976 by Alvarez and Macovski [35,36]. Over the past few decades, similar physics principles from dual-energy radiography were applied to CT through various technical applications. A number of DECT approaches have been validated and deployed in the clinical environment (Movie 1). Broadly, these may be grouped into emission versus detector-based techniques [37–41], with major differences highlighted in Table 1.

There are multiple image types, and reconstructions that may be obtained from DECT scanner regardless of the dual-energy approach. Some of the most commonly generated image reconstructions from dual-energy CT include virtual mono-energetic images (VMI), virtual non-contrast images (VNC), iodine density map images, and Z-effective images (Table 3). The attenuation maximum occurring at the k-edge of iodine is the underlying principle which is exploited in low keV virtual monoenergetic imaging, while a high keV VMI may assist with metal or other beam-hardening artifact reduction. VNC images resemble unenhanced acquisitions without additional dose and allow for better characterization of incidental findings [42]. The iodine density map images also utilize DECT's ability to identify iodine but instead provide a map with quantification of iodine density throughout the images [43]. These may also be generated as a color-coded overlay on conventional CT images. Finally, Z-effective images create a color-coded map that stratifies relative material atomic numbers in each voxel relative to the conventional CT images.

## 7. Workflow considerations with DECT

The cardiothoracic DECT workflow relies most heavily on the VNC, low keV VMI, and iodine density map images (Fig. 7). In general, cardiothoracic studies should all include some combination of the aforementioned DECT reconstructions as standard to ensure that the most clinical data is acquired from a single exam [44,45]. For maximized clinical adoption and radiologist efficiency, the best performing workflow at our institution is incorporating these reconstructions into the existing protocols and enabling automatic transfer from scanner to PACS. This allows for seamless integration of DECT into the radiologist's traditional workflow with minimal interruption and the additional DECT images immediately available for reference (Supplemental Fig. 1).

## 8. Benefits and clinical applications of DECT

There are numerous advantages and benefits for using dual-energy CT in cardiothoracic applications (Table 4). When combined with the standard conventional CT images, the combination of DECT images ultimately aid the radiologist in appropriate diagnosis and evaluation of cardiothoracic disease.

### 8.1. Better diagnostic certainty

Several studies have shown that the utilization of DECT adds value with an increase in a radiologist's diagnostic certainty and confidence for a variety of clinical applications [40,41,46]. In cardiothoracic imaging, detection of pulmonary emboli has been one of the earliest validated strengths of DECT regardless of the approach [47]. Some

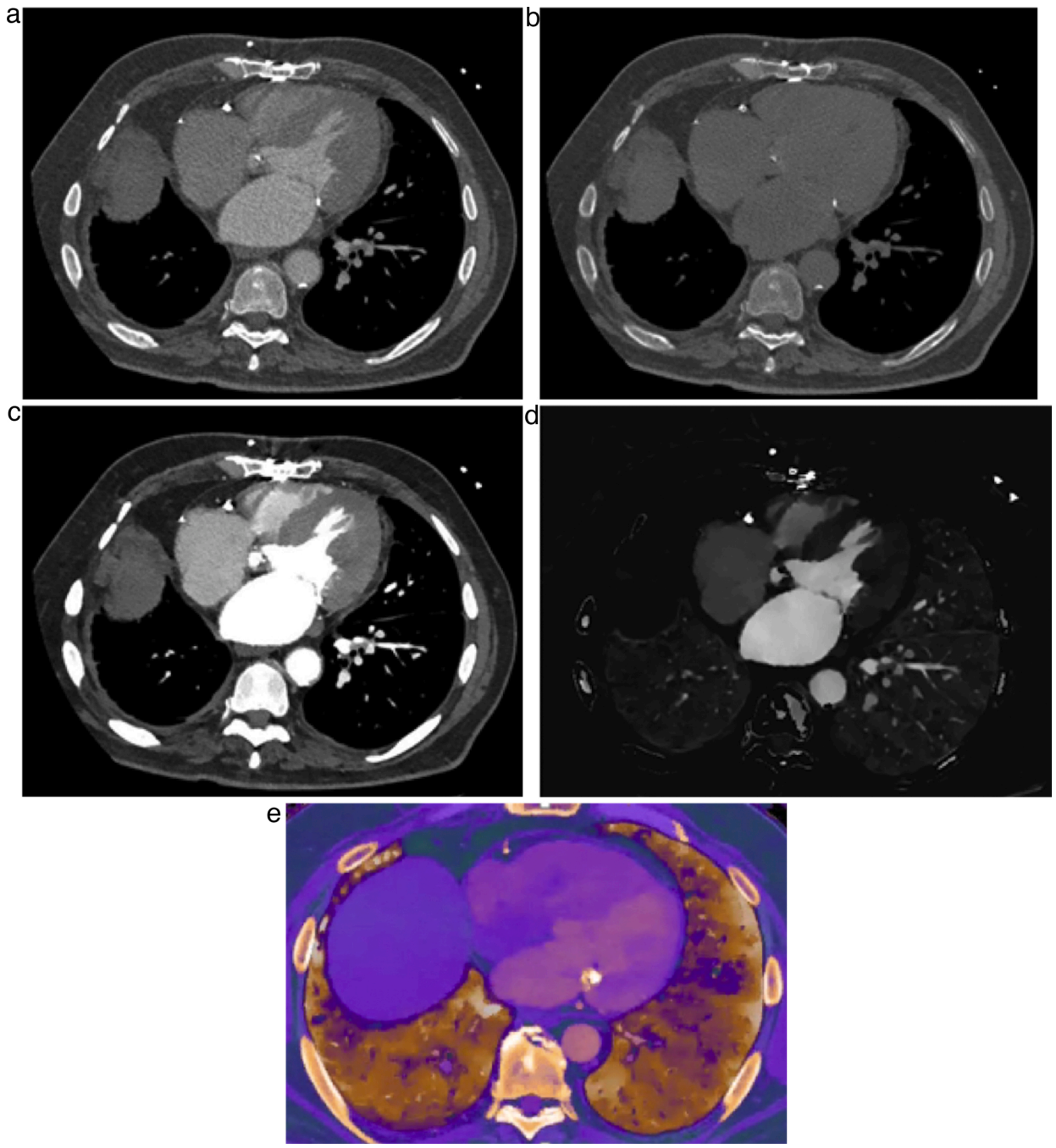


**Fig. 7.** Most useful DECT reconstructions for routine clinical cardiovascular applications. (a) Conventional CT image, similar to routine CT image, providing a starting point for assessment (b) Virtual non contrast image, obtained by removal of iodine from contrast enhanced image, can serve as a surrogate for true non contrast image (c) Low keV images, provide contrast boost because of increased attenuation, resulting in better depiction of contrast enhancement (d) Iodine density image, demonstrates the distribution of iodinated contrast and can be used for lesion characterization and organ perfusion and allows for quantification of enhancement, (e) Overlay image, combines anatomical information of CT with iodine distribution; can be used instead of iodine density images.

additional validated cardiothoracic applications include myocardial perfusion, myocardial ischemia, aortic disease, endoleak, and pulmonary perfusion defects [41,46]. Recent studies have shown that pulmonary angiography on newer DECT scanners results in improved subjective and objective image quality without increased radiation exposure as compared to older generation DECT scanners and standard CT image acquisition [48,49]. By using a combination of low keV virtual monenergistic images to boost contrast enhancement as well as iodine density map images to visualize and quantify enhancement, pulmonary perfusion defects of pulmonary arterial or venous origin that may have been missed on an initial screening are better detected (Fig. 8) [50]. The image quality and diagnostic confidence can be further enhanced by optimizing window and level settings of the VMI [51,52]. Okada et al. have shown that inter- and intraobserver agreement is increased in pulmonary embolism studies with DECT iodine density map images compared to those with conventional CT alone (Az = 0.966 [reader 1] and 0.959 [reader 2] compared to Az = 0.888 [reader 1] and 0.912 [reader 2], $p < 0.001$) [53]. Additionally, early studies have demonstrated that quantitative data from iodine density map perfusion images inversely correlates with a patient's pulmonary embolism thrombus load and may be a surrogate marker to gold standard laboratory values and cardiac strain for determining the severity of an acute pulmonary

**Table 4**
Summary of Dual-Energy CT Applications in Cardiothoracic Disease.

| Benefit | Most useful DECT Reconstruction | Clinical Utility and Advantages |
|---|---|---|
| Increased Diagnostic Confidence and Time Saving | VMI (Low and high energies)<br>VNC<br>Iodine Density Map Images | Improved workflow for detecting vascular abnormalities (Pulmonary Embolism)<br>Confident differentiation of calcium, iodine, and other materials |
| Improve Contrast Enhancement | VMI (Low energy) | Salvage missed contrast bolus exam<br>Improve contrast attenuation for diagnosis<br>Eliminate need for repeat exam in conventional suboptimal CT<br>Reduced contrast volume bolus |
| Artifact Reduction | VMI (High Energy) | Improve or resolve metallic and other beam-hardening CT artifacts<br>Eliminate need for repeat exam |
| Lesion detection & characterization | VNC<br>VMI (Low and high energies)<br>Iodine Density Map Images | Quantify level of true lesion enhancement<br>Differentiate benign versus malignant intrathoracic lesions and other incidental findings |
| Radiation Dose Reduction | VNC<br>VMI (Low energy) | Eliminate need for true non-enhanced CT for lesion detection<br>Single phase examination on DECT can provide information similar to multiphase CT<br>Salvage exam diagnosis through improved contrast attenuation |
| Estimate Organ Function | Iodine Density Map Images<br>VNC | Enable quantification of lung perfusion which is surrogate for function.<br>Assessment of myocardial perfusion defects and myocardial scarring/fibrosis. |

embolism ($r = -0.46$; $p < 0.001$) [46]. Also, a perfusion defect on iodine density map images with patent pulmonary arteries guides the radiologist toward searching for an alternate cause for the perfusion defect such as extraneous compression of pulmonary arteries, or airway compromise (Supplemental Fig. 2).

### 8.2. Boost contrast enhancement/reduction in contrast use

Low keV VMI from DECT increases the attenuation of iodinated contrast material allowing for increased CT contrast enhancement. Retrospective application of this principle includes salvaging an exam where the contrast bolus was mistimed or limited in amount. By accessing the low keV VMI, a non-diagnostic vascular study may become diagnostically acceptable and a patient may be spared from repeat examination with additional radiation exposure and more contrast (Fig. 9). This is essential in rapid care or emergency settings as well as outpatient environments where downtime or repeat studies carry a significant time and economic penalty. Some institutions have implemented prospective protocols that take advantage of this concept through decreased contrast dose volume as a standard of care [54,55]. The focus of these interventions has been centered on those patients where a contrast-enhanced CT is beneficial or necessary in the setting of renal impairment such as pre-operative evaluation for transcatheter aortic valve implantation (TAVI) or other vascular intervention (Fig. 10). Here the improved SNR of the low keV images is used to reduce the dose of nephrotoxic intravenous contrast without loss of vascular contrast or radiation exposure, particularly important in scanning patients with renal insufficiency [56]. With DECT, patients who may not have been offered these interventions before, given the amount of contrast needed for imaging, may have a chance for proper imaging evaluation and risk stratification prior to clinical decision making.

### 8.3. Beam hardening artifact reduction

High keV VMI from DECT allows for reduction of beam hardening and metal artifacts that traditionally may limit conventional CT interpretation. Typical cardiothoracic artifacts originate from x-ray beam interactions with metallic medical hardware in the chest wall, cardiac, or osseous structures resulting in dark spots or streaks over adjacent critical anatomical structures. Since these medical devices are usually fixed in location, the associated artifacts will be most severe closest to the hardware but may extend through an entire CT slice depending on the severity. If critical anatomy or pathology is obscured by the hardware artifact, it will limit the diagnostic certainty of the radiology or simply be missed. While advances in conventional CT have offered some support in limiting these artifacts through post-processing algorithms, studies have shown that combining DECT data with these conventional CT algorithms may further improve study quality [57]. Similar to boosting contrast enhancement with low keV images, the artifact reduction from high keV images may salvage an otherwise non-diagnostic exam and save the patient from additional radiation dose from a repeat CT (Fig. 1b).

### 8.4. Improved lesion detection/characterization

DECT material decomposition properties provide a distinct advantage over conventional CT for detection and characterization of cardiothoracic pathologies. For instance, DECT iodine density map images can qualitatively and quantitatively identify iodine beyond traditional HU attenuation characteristics alone. Through iodine density map overlay images, these findings may be anatomically correlated for further characterization. Common benefits of DECT reconstructions in cardiothoracic imaging include tumor recurrence in surgical or radiation fields, benign verwsus malignant incidental lesions, and early detection of malignancy (Fig. 11) [50,58–60]. Early studies have also demonstrated how DECT may be used as an early detector for tumor recurrence after radiofrequency ablation of lung malignancies [61]. Additionally, VNC images from DECT may replace true unenhanced conventional CT images and allows for improved assessment of calcified or non-enhancing nodules/lesions (Fig. 12). This provides imaging information that would otherwise require additional radiation dose as well as increased scan time using conventional CT only.

### 8.5. Incidental lesion assessment

Most chest CT protocols incorporate portions of the lower neck and upper abdomen, and radiologists are expected to identify incidental imaging findings in this location. Conventional CT of the chest also does not optimize contrast bolus timing for appropriate evaluation of these areas and therefore the lesions are often labelled as indeterminate. Despite the limited field of view, utilization of DECT over conventional CT may help in definitive characterization of many of the lesions reducing the need for additional dedicated imaging. This may include renal, hepatic, adrenal, pancreatic, or osseous lesions. For example, Wortman et al. reviewed how DECT VMI may increase conspicuity of incidental lesions identified in the liver or pancreas compared to those found on conventional CT alone [62]. A VNC image may be used as a surrogate for dual phase conventional CT and help characterize a lipid-rich adenoma [63]. Incidental hypoattenuating/hyperattenuating hepatic or renal cysts often present a diagnostic dilemma in patients with work up for metastatic disease. Conventional CT characteristics such as size and attenuation may not always be enough to provide a

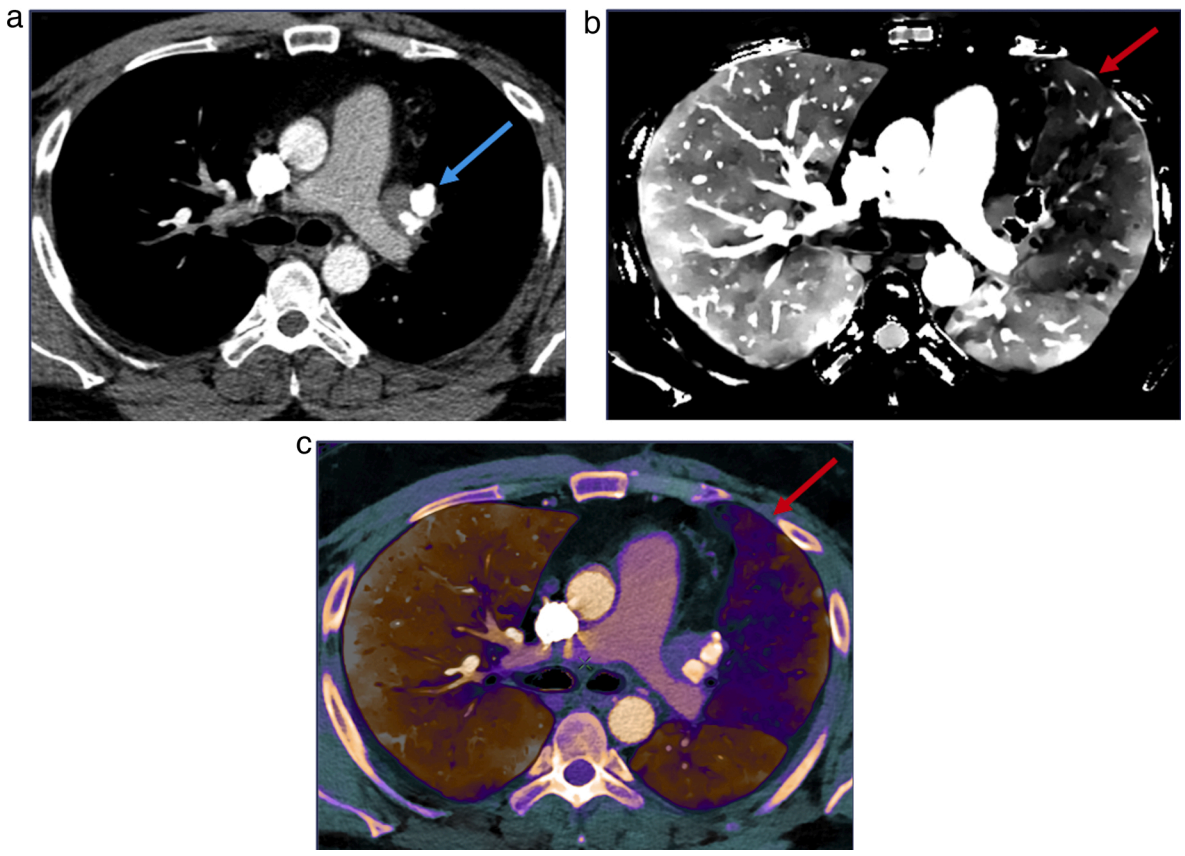


**Fig. 8.** Better diagnostic certainty with DECT. A 38-year-old male with history of annual episodes of massive hemoptysis, which has been going on for several years and resolved each time with antibiotics and steroids and cough suppression. Initial axial conventional CT image (a) demonstrate a partially calcified mass within left aspect of the mediastinum (Arrow) at the expected location of left superior pulmonary vein (vein not visualized). The iodine density (b) and overlay images (c) demonstrate a large perfusion defect of the left upper lobe lung (Arrows), in the distribution of left superior pulmonary vein. Given the patent pulmonary arteries and above-mentioned findings, diagnosis of pulmonary venous occlusion secondary to granulomatous disease was considered.

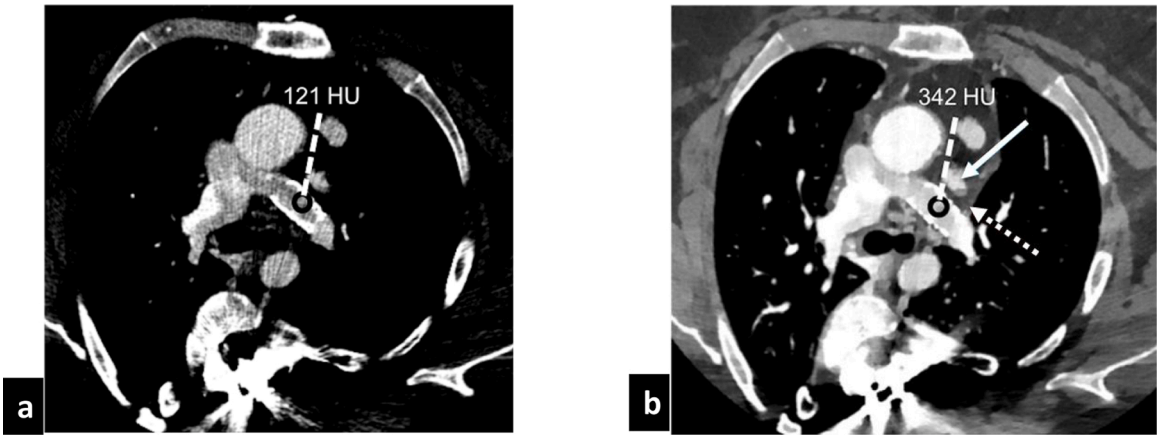


**Fig. 9.** Contrast boost by low keV VMI. A 32-year-old female, with a history of tricuspid atresia, status post left BT shunt in the newborn period, status post classic Fontan followed by fenestrated Fontan and subsequent left pulmonary artery reconstruction and placement of permanent pacemaker. The patient now presents with acute chest pain. Initial conventional CT image (a) demonstrate very poor opacification of the pulmonary arteries and a suspected filling defect/ embolus within the stented left main pulmonary artery. The low keV VM image (b) from the same exam provides the contrast boost and therefore diagnosis of sluggish flow within left pulmonary artery, secondary to the left superior pulmonary vein occlusion was made (Please note that left superior pulmonary vein is not visualized- consistent with chronic occlusion- Red arrow indicates expected location of left superior pulmonary vein and blue arrow represents a portion of left atrial appendage).

confident benign versus suspicious diagnosis. DECT images, particularly iodine density map images, may further identify true iodine uptake in these incidental lesions and serve as a surrogate marker for recommending further workup (Fig. 13).

### *8.6. Estimation of organ function*

Iodine density map images from DECT may be directly correlated with estimated organ function and perfusion. This property has proven useful in pre- and post-operative therapy planning and assessment. For

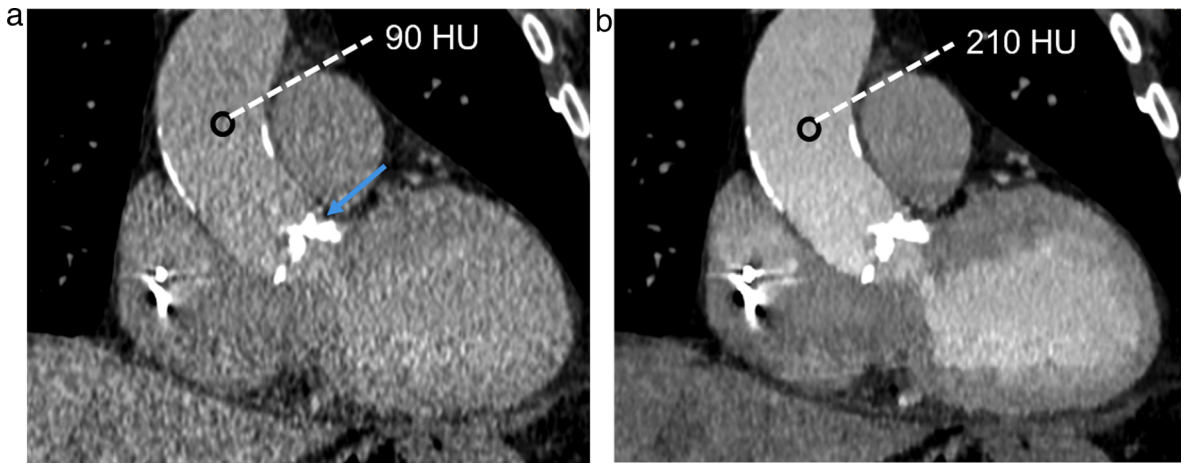


**Fig. 10.** Contrast dose reduction with DECT. A 72-year-old male with history of renal dysfunction (eGFR =30 mL/min/1.73m2) comes for Pre – TAVI (Transcatheter Aortic valve Implantation) planning scan. (a) Conventional coronal CT image from DECT scan following intravenous administration of 25 mL of iodinated contrast shows poor contrast opacification of thoracic aorta. (b) Low keV VM image provides necessary contrast boost making the examination diagnostic at a very low contrast dose (as compared to 70-90 ml with conventional CT). Of note dense aortic valve calcification correlate with patient's severe aortic stenosis (Arrow in a).

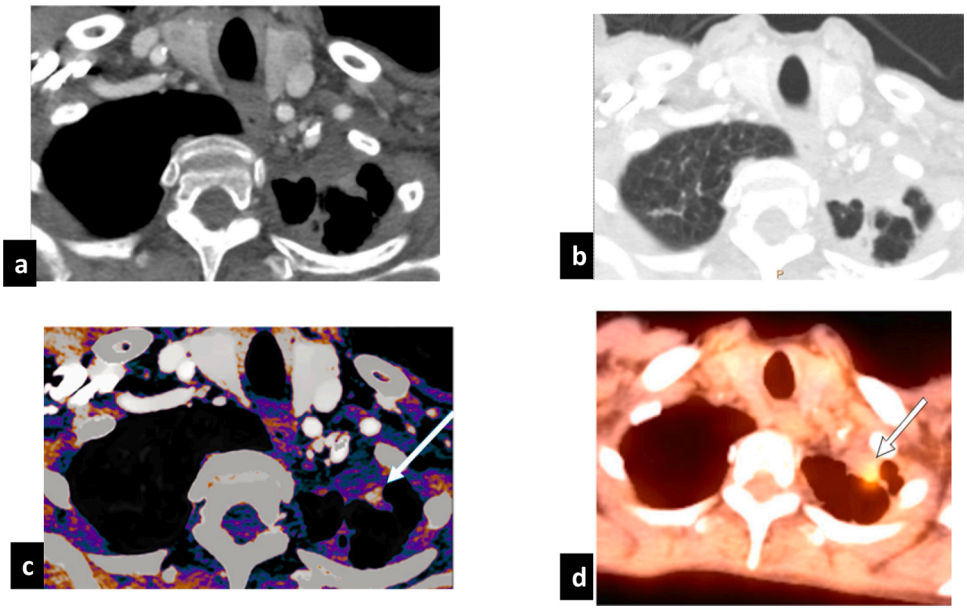


**Fig. 11.** Improved lesion detection with DECT. A 79-year-old female with history of left upper lobe adenocarcinoma status post resection and radiation therapy returning for restaging scan. On conventional CT images in soft tissue and lung window settings (a, b), there is left apical post-surgical scarring seen without definite local recurrence. However, on iodine overlay image (c) there is focus of increased iodine accumulation within the scarring (Blue arrow), which correspond to increased radiotracer uptake on subsequent PET-CT fusion image (Red arrow in d). Pathology confirmed recurrent adenocarcinoma.

example, where non-specific dense consolidation may limit diagnosis in a complex lung transplant patient, Hokamp et al. demonstrated that the iodine density map images with a lack of perfusion confirming the diagnosis of acute transplant rejection [64]. For pre-operative planning in cardiothoracic surgeries, DECT may include additional clinical data such as surrogate markers for cardiac perfusion which may redirect or alter management (Fig. 14). Rubinshtein et al. showed that DECT myocardial perfusion imaging demonstrated high specificity (98 %) and negative predictive value (99 %) for detection of myocardial infarction when compared to the gold standard of Technetium [99mTc]-Sestamibi single photon emission computed tomography (SPECT) [65]. Similarly, Carrascosa et al. demonstrated that stress myocardial perfusion protocol by DECT added value in detecting reversible perfusion defects ((area under ROC curve 0.84 (0.80−0.87)) and anatomy of coronary artery disease (area under ROC curve 0.70 (0.65−0.74)) compared to SPECT and CT coronary angiography, respectively [66]. In radiation therapy planning, studies have demonstrated that average iodine density of tumor from DECT may serve as a noninvasive and quantitative assessment of radio-resistance and predictor of the prognosis and overall treatment response [67].

### 8.7. Reduction in radiation dose

Most literature confirms that modern DECT scanners are able to achieve equal or decreased radiation doses delivery compared to conventional CT [68]. Lenga et al. specifically investigated second and third-generation DECT compared to conventional single energy CT in imaging of the chest and found no significant increase in radiation dose as well as no significant decrease in image quality [68]. Bauer et al. shared the same findings for first and second generation DECT compared to single-energy CT in CT pulmonary angiography [69]. DECT manufacturers all include up-to-date CT dose-reduction techniques as well as streamlined protocoling for equivalent or improved SNR. Furthermore, VNC may be considered equivalent to true non-contrast conventional CT images enabling streamlined DECT single-phase acquisition versus previously required multiphase single-energy conventional CT, allowing for significant radiation dose reduction (Fig. 15). Utilization of VMI may also salvage suboptimal exams as well as reduce CT artifacts eliminating

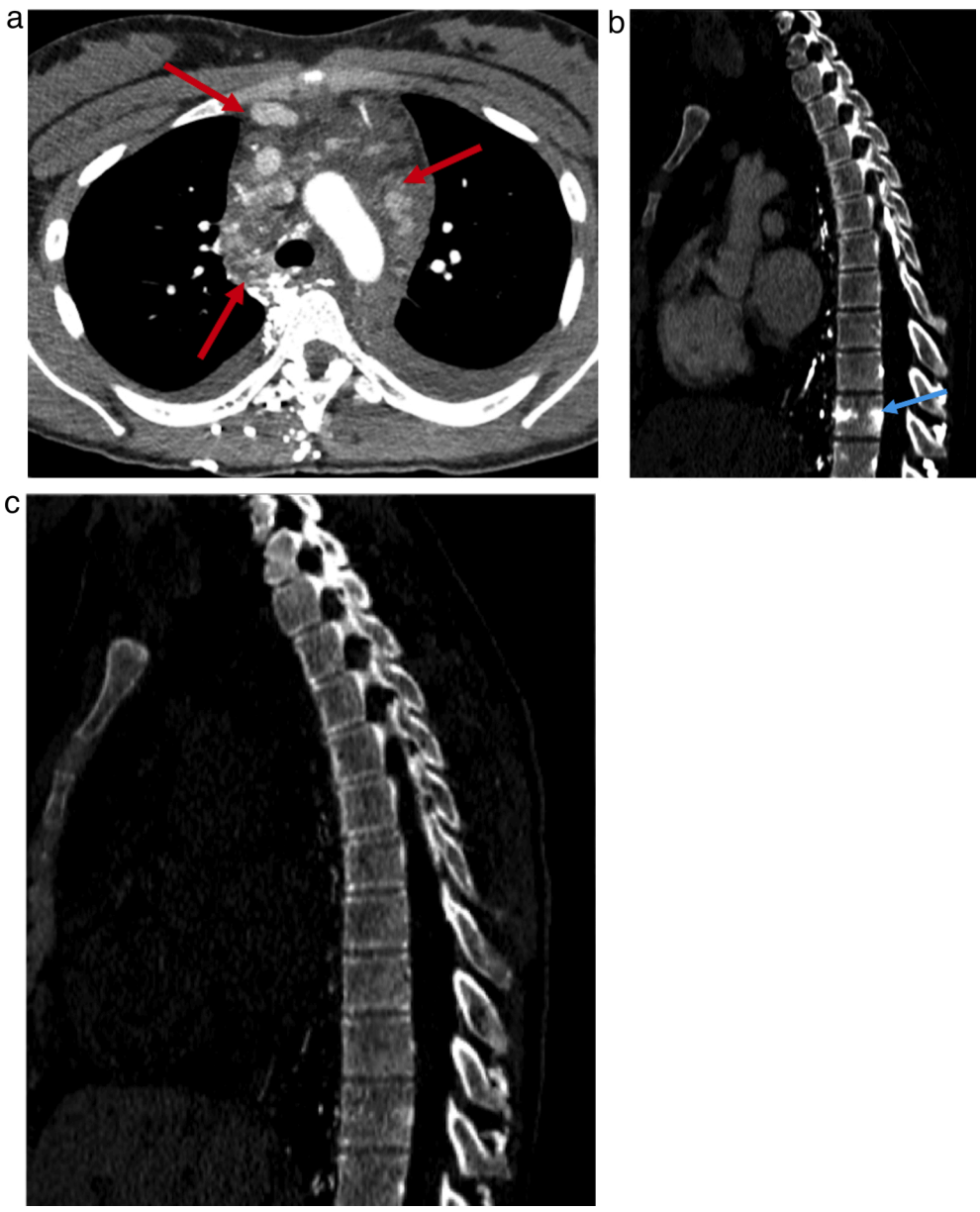


**Fig. 12.** Better lesion characterization with DECT. A 74-year-old male with prior history of mediastinal mass consistent with small cell cancer, status post chemoradiotherapy. Initial conventional CT image (a) shows nonspecific fat stranding and soft tissue density in mediastinum, consistent with combination of tumor and post therapy changes. In addition, there is extensive collateralization in the mediastinum secondary to patients known Superior Vena Cava (SVC) involvement (Arrows in a). There is a new ill-defined hyperdense lesion seen in lower thoracic spine on conventional CT (Aarrow in b), which is indeterminate for metastatic disease. However, the vertebral lesion disappears on VNC image(c) pointing towards intraosseous enhancement secondary to SVC syndrome and not neoplastic lesion.

the need for a repeat CT for a diagnosis.

### 8.8. Emerging clinical indications

Research and experimentation in emerging applications and utility for DECT continues to grow. In radiation therapy treatment planning, Lapointe et al. found that iodine pulmonary perfusion DECT images strongly correlated with SPECT for differential function per lobe calculations (Pearson's coefficient r = 0.91) [70]. Future cardiothoracic applications of DECT are promising including the use of DECT for pulmonary lesion evaluation and lobar functional assessment in a single study, obviating the need for an additional SPECT-CT [71]. Coronary calcium scoring CT has expanded in clinical practice and the combination of DECT with VNC images for definitive calcium identification and subtraction may further enhance the clinical value. (Supplemental Fig. 3). Medical 3D printing commonly uses CT as the source for anatomic segmentation and using DECT images improves the medical 3D printing workflow over conventional CT [72]. Additionally, the combination of contrast enhancing properties from low keV VMI and artifact reduction from high keV VMI improves the ability of automated segmentation tools to threshold and differentiate critical anatomic structures for 3D printing (Supplemental Fig. 4) [72].

## 9. Future directions

### 9.1. Integrated PET/dual energy CT

Positron Emission Tomography (PET) fused with a conventional CT is commonly implemented with multiple use cases in molecular and functional imaging. The fusion of CT with PET imaging allows precise alignment of metabolic activity in the body obtained by PET with anatomical imaging obtained by CT. The use of PET/CT has led to improved diagnosis and determination of treatment response in the fields of oncology and radiation therapy [73,74]. As compared to conventional CT, DECT techniques allow for the quantitative characterization of tissue composition. Thus, the combination of DECT with PET imaging allows for a more comprehensive characterization of diseases than DECT or PET/CT alone. This couples the quantitative tissue characterization afforded by the DECT with molecular information from the PET [75].

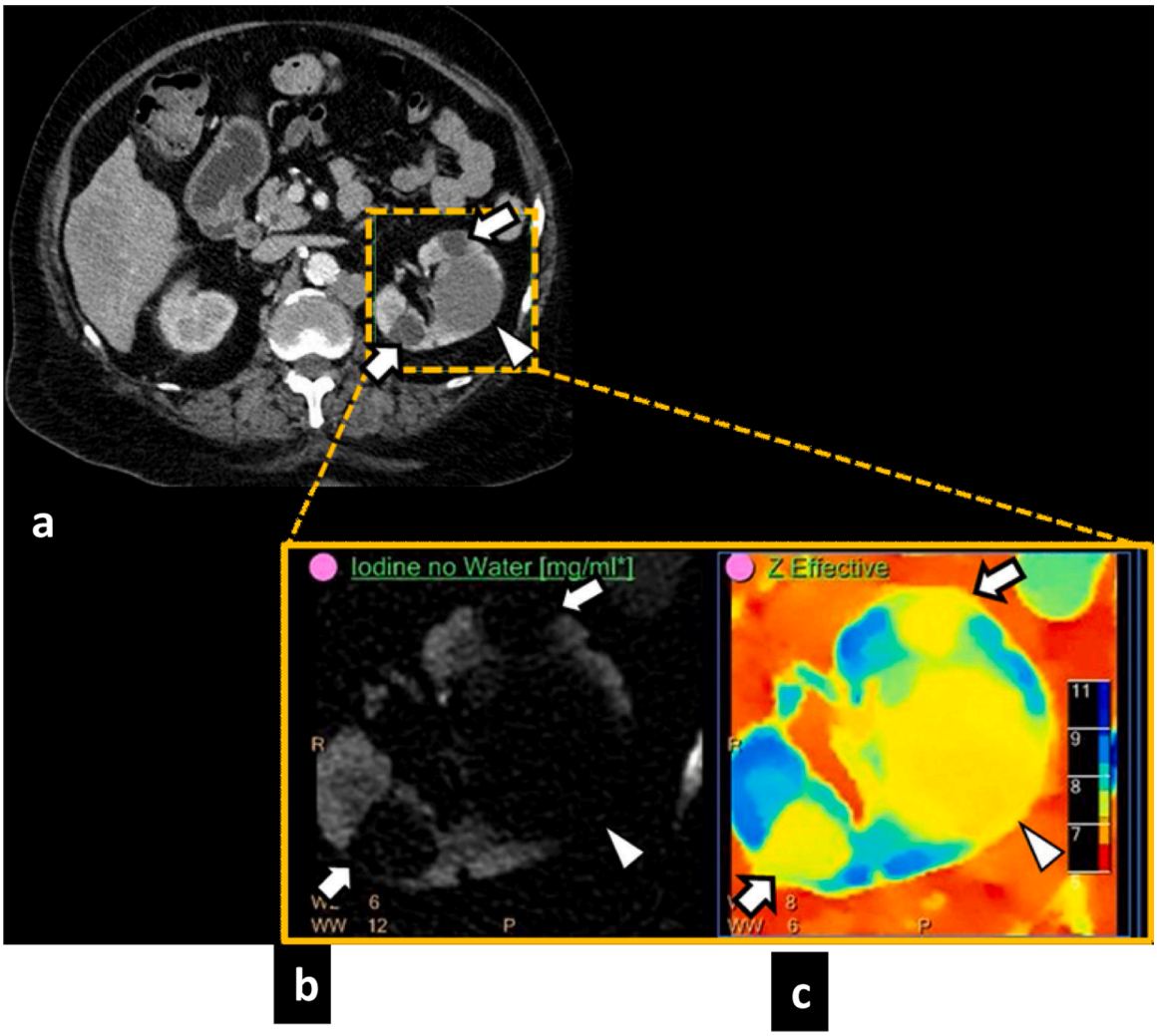


**Fig. 13.** Incidental lesion assessment with DECT. A 80-year-old male was scanned as part of the pre TAVI (Transcatheter Aortic Valve Implantation) work up. Axial CT image (a) demonstrate incidentally noted hypodense (white arrows) and hyperdense left renal lesions(blue arrow), which were without iodine accumulation on iodine density (b)and Z effective images(c), consistent with hemorrhagic and non-hemorrhagic renal cysts.

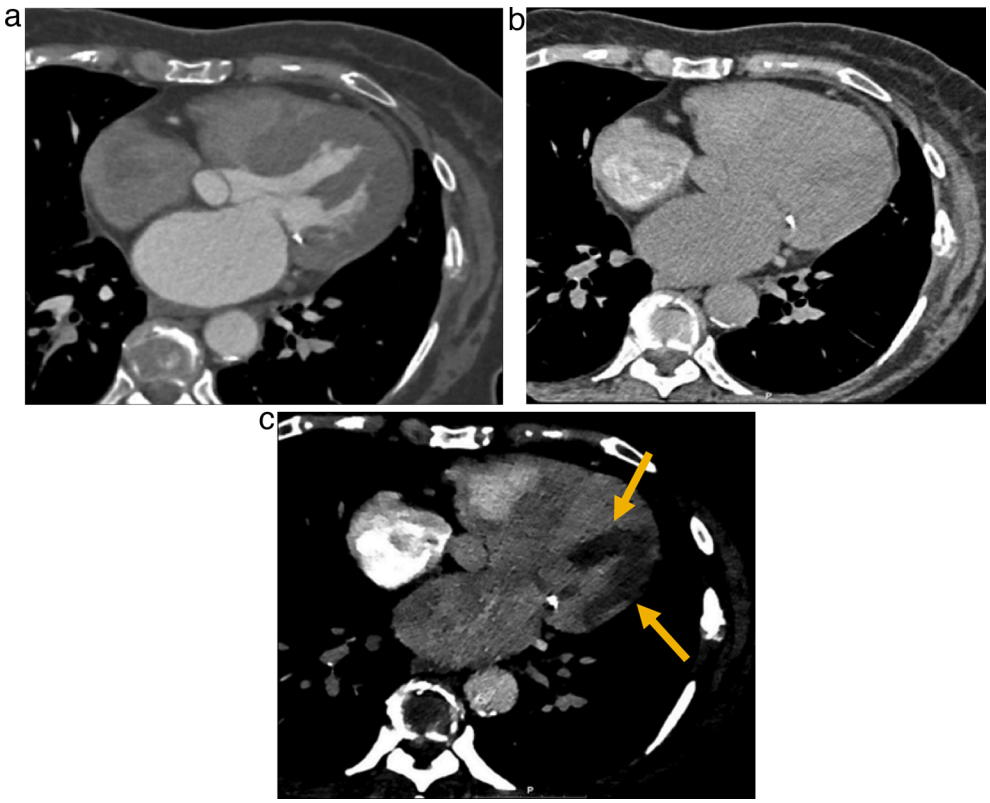


**Fig. 14.** Assessment of myocardial perfusion on DECT. A 81-year-old woman with history of chronic atrial fibrillation was planned for a left atrial appendage occlusion procedure. A planning cardiac CT; Early (a) and delayed conventional CT images (b) were unremarkable, however there was a clear large perfusion defect(Arrows), consistent with infarction, seen involving lateral left ventricular myocardium and papillary muscle on low keV VM image from delayed scan (c). Subsequent cardiac catheterization revealed total occlusion of the first obtuse marginal branch of the left circumflex coronary artery (not shown).

However, this integration is fraught with several challenges. If the single-energy CT scanners were replaced by DECT, it would require a new higher cost scanner. While existing CT scanners can be retrofitted to allow dual-energy applications, there would be increased radiation dose and scanning expenses. Research by Wang et al. focused on devising novel methodologies to use available PET data from PET/CT to construct an integrated PET/DECT method without the need for additional hardware or radiation exposure [76].

### 9.2. *Photon counting CT*

Photon counting CT is multi-energy CT technique, currently being developed, which employ a photon-counting detector to register the interaction of individual photons [77]. The detector pixels estimate the energy in each individual photon interaction and record an approximate energy spectrum. Conventional CT scanners with energy-integrating detectors only record photon intensity while photon counting CTs also register additional spectral information. This provides improved SNR with better correction of beam-hardening artefacts, reduced radiation exposure, and improved spatial resolution (Fig. 16) [78]. It also provides the ability to distinguish multiple contrast agents. Presently, photon counting CTs are in experimental and research use at three sites in the world including the National Institute of Health (NIH) Clinical Center [79]. Current technical limitations have yet to be overcome such as a limited overall count rate, slower gantry movement to acquire enough photons, and polarization. Additionally, there are a multitude of manufacturing challenges and high costs associated with this technology.

### 9.3. *AI in dual energy CT analysis*

Artificial Intelligence (AI) methods which includes machine- and deep-learning techniques have recently shown increasing promise in interrogating subtle sub-visual clues on conventional radiology and pathology images. This includes detection, diagnosis, prognosis, and treatment response especially in cancer. AI methods are reliant on the spatial resolution and image SNR [80–82]. Dual-energy techniques result in images with increasing amounts of quantifiable data and improved SNR which are therefore well suited to address the needs of AI analyses. The relative lack of widespread clinical adoption of dual-energy radiography and CT techniques has meant that research in AI and dual-energy image analysis is currently limited. Seidler et al. used radiomic textural analysis on virtual monochromatic image (VMI) from DECT imaging of the neck from 50 patients having a total of 412 lymph nodes to differentiate benign from malignant lymph nodes [83]. The accuracy, sensitivity, specificity, PPV, and NPV for correctly classifying a lymph node as malignant (i.e. metastatic Head and neck Squamous cell cancer or lymphoma) versus benign were 92 %, 91 %, 93 %, 95 %, 87 %, respectively.

## 10. Conclusion

Dual-energy radiography and CT are powerful clinical tools for evaluating a wide range of cardiothoracic diseases. Through an understanding of the basic physics and the common dual energy images/reconstructions available, radiologists and clinicians may increase their confidence with cardiothoracic findings and avoid pitfalls associated with interpreting dual energy imaging data.

## Disclosures

Robert C Gilkeson, MD discloses research support from Philips Medical, General Electric, Siemens and consultant for Riverain Medical and Heartflow.

Amit Gupta, MD discloses research support from General Electric

Rest of the authors have nothing to disclose.

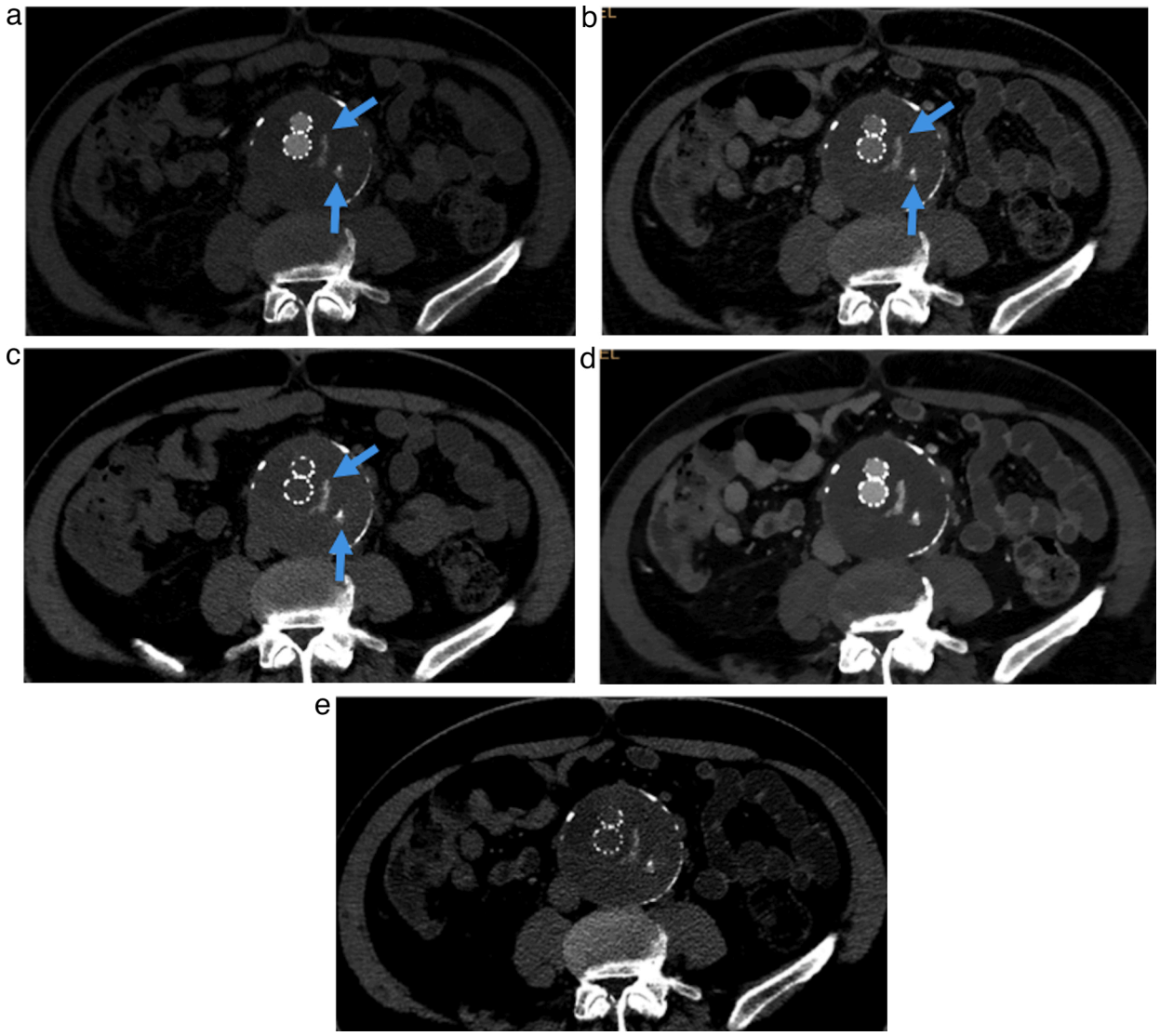


**Fig. 15.** Radiation dose reduction with DECT. A 64-year-old male with history of endovascular aneurysm repair (EVAR) for abdominal aortic aneurysm (AAA), underwent a follow up three phase CT angiogram (non-contrast, arterial phase and delayed phase scanning) of the abdomen and pelvis. Axial arterial phase image (a) demonstrates areas of hyperattenuation outside the stent in the excluded abdominal aortic aneurysm (Arrows), which persists on true non-contrast (TNC) image(c) and does not change on delayed contrast enhanced image (b). The findings are consistent with calcification in the excluded AAA and not an endoleak. When utilizing the low keV VM image (d) and VNC (e) reconstructions from the single delayed phase examination (b), comparable information to a three-phase scan can be obtained, thus, there is a potential of significantly reducing radiation exposure to the patient.

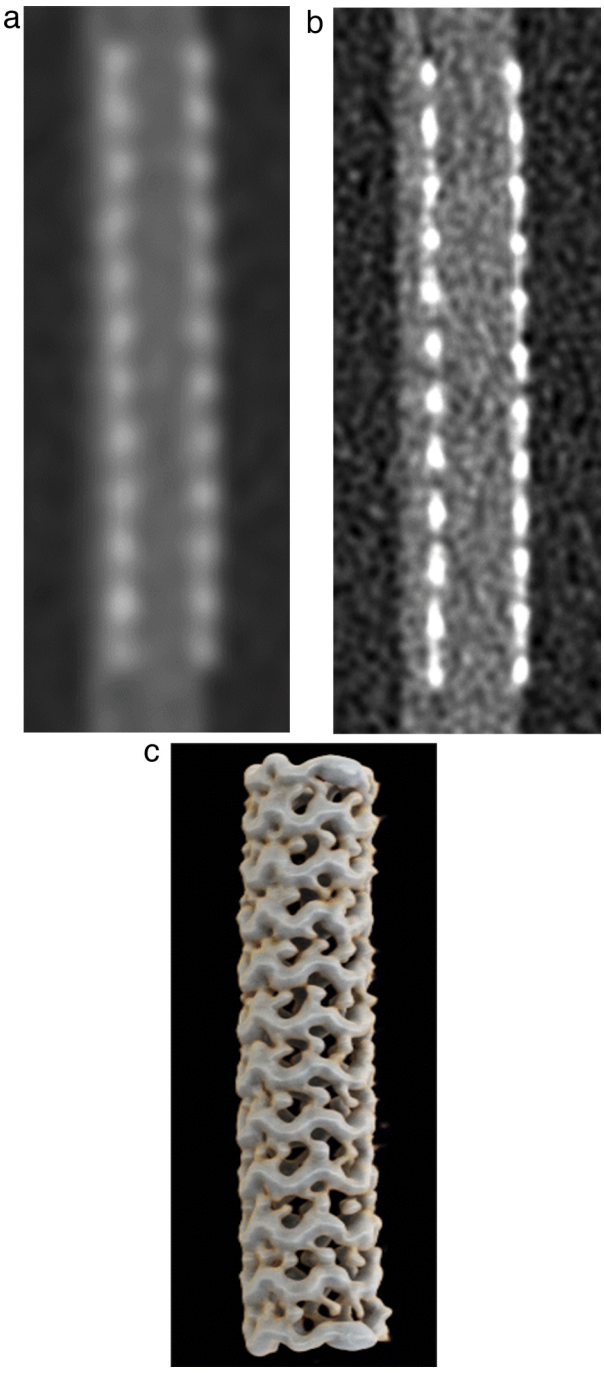


**Fig. 16.** Superior image quality with Photon-counting detector (PCD) CT. Coronal conventional CT (a) and PCD CT image (b) acquired in ultra-high resolution mode demonstrate better spatial resolution and delineation of coronary stent struts on PCD CT image, enabling reconstruction of a detailed three-dimensional volume rendered image(c).
Images (Fig. 9a, 9b and 9c in original paper) reprinted with permission from S. Leng, M. Bruesewitz, S. Tao, K. Rajendran, A.F.Halaweish, N.G. Campeau, J.G. Fletcher, C.H. McCollough, Photon-counting Detector CT: System Design and Clinical Applications of an Emerging Technology. Radiographics. 39(3) (2019) 729–743.

## Ethical statement

There are no ethical issues associated with this review paper.
There are no human or animal experiments involved in this study.
The authors received waiver of consent for this retrospective project by the institutional review board

## Funding statement

This research did not receive any specific grant from funding agencies in the public, commercial, or not-for-profit sectors.

## Declaration of Competing Interest

The author(s) or author(s) institutions have no conflicts of interest pertaining to this project.

## Appendix A. Supplementary data

Supplementary material related to this article can be found, in the online version, at doi:https://doi.org/10.1016/j.ejro.2021.100324.

## References

[1] M. Takai, M. Kaneko, Discrimination between thorotrast and iodine contrast medium by means of dual-energy CT scanning, Phys. Med. Biol. 29 (8) (1984) 959–967.
[2] F. Kelcz, P.M. Joseph, S.K. Hilal, Noise considerations in dual energy CT scanning, Med. Phys. 6 (5) (1979) 418–425.
[3] Y. Yao, J.M. Ng, A.J. Megibow, N.J. Pelc, Image quality comparison between single energy and dual energy CT protocols for hepatic imaging, Med. Phys. 43 (8) (2016) 4877.
[4] T. Heye, R.C. Nelson, L.M. Ho, D. Marin, D.T. Boll, Dual-energy CT applications in the abdomen, AJR Am. J. Roentgenol. 199 (5 Suppl) (2012) S64–70.
[5] H.W. Goo, J.M. Goo, Dual-energy C.T.: new horizon in medical imaging, Korean J. Radiol. 18 (4) (2017) 555–569.
[6] C.A. Coursey, R.C. Nelson, D.T. Boll, E.K. Paulson, L.M. Ho, A.M. Neville, D. Marin, R.T. Gupta, S.T. Schindera, Dual-energy multidetector CT: how does it work, what can it tell us, and when can we use it in abdominopelvic imaging? Radiographics 30 (4) (2010) 1037–1055.
[7] M. Rosenstein, Organ Doses in Diagnostic Radiology, 1976.
[8] H.E. Johns, J.R. Cunningham, The Physics of Radiology, 1983.
[9] M.C. Godoy, D.P. Naidich, E. Marchiori, B. Assadourian, C. Leidecker, B. Schmidt, I. Vlahos, Basic principles and postprocessing techniques of dual-energy CT: illustrated by selected congenital abnormalities of the thorax, J. Thorac. Imaging 24 (2) (2009) 152–159.
[10] C. van Kuijk, J.L. Grashuis, J.C. Steenbeek, H.E. Schutte, W.T. Trouerbach, Evaluation of postprocessing dual-energy methods in quantitative computed tomography. Part 2. Practical aspects, Invest. Radiol. 25 (8) (1990) 882–889.
[11] M.R. Lemacks, S.C. Kappadath, C.C. Shaw, X. Liu, G.J. Whitman, A dual-energy subtraction technique for microcalcification imaging in digital mammography–a signal-to-noise analysis, Med. Phys. 29 (8) (2002) 1739–1751.
[12] P. Vock, Z. Szucs-Farkas, Dual energy subtraction: principles and clinical applications, Eur. J. Radiol. 72 (2) (2009) 231–237.
[13] T. Ishigaki, S. Sakuma, M. Ikeda, One-shot dual-energy subtraction chest imaging with computed radiography: clinical evaluation of film images, Radiology 168 (1) (1988) 67–72.
[14] T. Ishigaki, S. Sakuma, Y. Horikawa, M. Ikeda, H. Yamaguchi, One-shot dual-energy subtraction imaging, Radiology 161 (1) (1986) 271–273.
[15] F. Fischbach, T. Freund, R. Rottgen, U. Engert, R. Felix, J. Ricke, Dual-energy chest radiography with a flat-panel digital detector: revealing calcified chest abnormalities, AJR Am. J. Roentgenol. 181 (6) (2003) 1519–1524.
[16] R. Kamimura, T. Takashima, Clinical application of single dual-energy subtraction technique with digital storage-phosphor radiography, J. Digit. Imaging 8 (1 Suppl 1) (1995) 21–24.
[17] S. Kido, K. Kuriyama, C. Kuroda, H. Nakamura, W. Ito, K. Shimura, H. Kato, Detection of simulated pulmonary nodules by single-exposure dual-energy computed radiography of the chest: effect of a computer-aided diagnosis system (Part 2), Eur. J. Radiol. 44 (3) (2002) 205–209.
[18] J.D. Balkman, S. Mehandru, E. DuPont, R.D. Novak, R.C. Gilkeson, Dual energy subtraction digital radiography improves performance of a next generation computer-aided detection program, J. Thorac. Imaging 25 (1) (2010) 41–47.
[19] Z. Szucs-Farkas, A. Schick, J.L. Cullmann, L. Ebner, B. Megyeri, P. Vock, A. Christe, Comparison of dual-energy subtraction and electronic bone suppression combined with computer-aided detection on chest radiographs: effect on human observers' performance in nodule detection, AJR Am. J. Roentgenol. 200 (5) (2013) 1006–1013.
[20] F. Li, R. Engelmann, C.E. Metz, K. Doi, H. MacMahon, Lung cancers missed on chest radiographs: results obtained with a commercial computer-aided detection program, Radiology 246 (1) (2008) 273–280.
[21] Z. Szucs-Farkas, M.A. Patak, S. Yuksel-Hatz, T. Ruder, P. Vock, Improved detection of pulmonary nodules on energy-subtracted chest radiographs with a commercial computer-aided diagnosis software: comparison with human observers, Eur. Radiol. 20 (6) (2010) 1289–1296.

[22] K. Martini, M. Baessler, S. Baumueller, T. Frauenfelder, Diagnostic accuracy and added value of dual-energy subtraction radiography compared to standard conventional radiography using computed tomography as standard of reference, PLoS One 12 (3) (2017), e0174285.
[23] G.J. Whitman, L.T. Niklason, M. Pandit, L.C. Oliver, E.H. Atkins, O. Kinnard, A. H. Alexander, M.K. Weiss, K. Sunku, E.S. Schulze, R.E. Greene, Dual-energy digital subtraction chest radiography: technical considerations, Curr. Probl. Diagn. Radiol. 31 (2) (2002) 48–62.
[24] J.E. Kuhlman, J. Collins, G.N. Brooks, D.R. Yandow, L.S. Broderick, Dual-energy subtraction chest radiography: what to look for beyond calcified nodules, Radiographics 26 (1) (2006) 79–92.
[25] A. Urbaneja, G. Dodin, G. Hossu, O. Bakour, R. Kechidi, P. Gondim Teixeira, A. Blum, Added value of bone subtraction in dual-energy digital radiography in the detection of pneumothorax: impact of reader expertise and medical specialty, Acad. Radiol. 25 (1) (2018) 82–87.
[26] J.T. Ho, R.A. Kruger, J.A. Sorenson, Comparison of dual and single exposure techniques in dual-energy chest radiography, Med. Phys. 16 (2) (1989) 202–208.
[27] H. MacMahon, W. Cannon, R. Engelmann, M. Carlin, K. Doi, Dual energy subtraction computed chest radiography: comparison of diagnostic accuracy with conventional computed radiography, Radiology 209 (1998) 544.
[28] R.C. Gilkeson, R.D. Novak, P. Sachs, Digital radiography with dual-energy subtraction: improved evaluation of cardiac calcification, AJR Am. J. Roentgenol. 183 (5) (2004) 1233–1238.
[29] O. Yamanaka, M. Sawano, R. Nakayama, M. Nemoto, T. Nakamura, Y. Fujiwara, S. Suzuki, Y. Hayashi, S. Yamagami, K. Minamisawa, A. Wada, N. Nyui, Clinical significance of coronary calcification, Circ. J. 66 (5) (2002) 473–478.
[30] J.N. Mafi, B. Fei, S. Roble, A. Dota, P. Katrapati, H.G. Bezerra, H. Wang, W. Wang, L. Ciancibello, M. Costa, D.I. Simon, C.E. Orringer, R.C. Gilkeson, Assessment of coronary artery calcium using dual-energy subtraction digital radiography, J. Digit. Imaging 25 (1) (2012) 129–136.
[31] C.M. Otto, B. Prendergast, Aortic-valve stenosis–from patients at risk to severe valve obstruction, N. Engl. J. Med. 371 (8) (2014) 744–756.
[32] R. Koos, H.P. Kuhl, G. Muhlenbruch, J.E. Wildberger, R.W. Gunther, A. H. Mahnken, Prevalence and clinical importance of aortic valve calcification detected incidentally on CT scans: comparison with echocardiography, Radiology 241 (1) (2006) 76–82.
[33] K. Ansari-Gilani, Y.K. Tandon, D.W. Jordan, L. Ciancibello, D.L. Wilson, R. C. Gilkeson, Dual-energy subtraction chest radiography: application in cardiovascular imaging, J. Thorac. Imaging (2020), https://doi.org/10.1097/RTI.0000000000000472.
[34] F. Kelcz, F.E. Zink, W.W. Peppler, D.G. Kruger, D.L. Ergun, C.A. Mistretta, Conventional chest radiography vs dual-energy computed radiography in the detection and characterization of pulmonary nodules, AJR Am. J. Roentgenol. 162 (2) (1994) 271–278.
[35] R.E. Alvarez, A. Macovski, Energy-selective reconstructions in X-ray computerized tomography, Phys. Med. Biol. 21 (5) (1976) 733–744.
[36] A. Macovski, R.E. Alvarez, J.L. Chan, J.P. Stonestrom, L.M. Zatz, Energy dependent reconstruction in X-ray computerized tomography, Comput. Biol. Med. 6 (4) (1976) 325–336.
[37] C.H. McCollough, S. Leng, L. Yu, J.G. Fletcher, Dual- and multi-energy CT: principles, technical approaches, and clinical applications, Radiology 276 (3) (2015) 637–653.
[38] K. Kalisz, S. Halliburton, S. Abbara, J.A. Leipsic, M.H. Albrecht, U.J. Schoepf, P. Rajiah, Update on cardiovascular applications of multienergy CT, Radiographics 37 (7) (2017) 1955–1974.
[39] J. Doerner, C. Wybranski, J. Byrtus, C. Houbois, M. Hauger, C. Heneweer, F. Siedek, T. Hickethier, N. Grosse Hokamp, D. Maintz, S. Haneder, Intra-individual comparison between abdominal virtual mono-energetic spectral and conventional images using a novel spectral detector CT, PLoS One 12 (8) (2017), e0183759.
[40] W.F. Wiggins, C.A. Potter, A.D. Sodickson, Dual-energy CT to differentiate small foci of intracranial hemorrhage from calcium, Radiology 294 (1) (2020) 129–138.
[41] S. Aran, L. Daftari Besheli, M. Karcaaltincaba, R. Gupta, E.J. Flores, H.H. Abujudeh, Applications of dual-energy CT in emergency radiology, AJR Am. J. Roentgenol. 202 (4) (2014) W314–24.
[42] C. Frellesen, M. Azadegan, S.S. Martin, K. Otani, T. D'Angelo, C. Booz, K. Eichler, B. Panahi, M. Kaup, R.W. Bauer, T.J. Vogl, J.L. Wichmann, Dual-energy computed tomography-based display of bone marrow edema in incidental vertebral compression fractures: diagnostic accuracy and characterization in oncological patients undergoing routine staging computed tomography, Invest. Radiol. 53 (7) (2018) 409–416.
[43] S.S. Martin, F. Trapp, J.L. Wichmann, M.H. Albrecht, L. Lenga, J. Durden, C. Booz, T.J. Vogl, T. D'Angelo, Dual-energy CT in early acute pancreatitis: improved detection using iodine quantification, Eur. Radiol. 29 (5) (2019) 2226–2232.
[44] L. Lenga, M.H. Albrecht, A.E. Othman, S.S. Martin, D. Leithner, T. D'Angelo, C. Arendt, J.E. Scholtz, C.N. De Cecco, U.J. Schoepf, T.J. Vogl, J.L. Wichmann, Monoenergetic dual-energy computed tomographic imaging: cardiothoracic applications, J. Thorac. Imaging 32 (3) (2017) 151–158.
[45] C.T. Arendt, R. Czwikla, L. Lenga, J.L. Wichmann, M.H. Albrecht, C. Booz, S. S. Martin, D. Leithner, P. Tischendorf, A. Blandino, T.J. Vogl, T. D'Angelo, Improved coronary artery contrast enhancement using noise-optimised virtual monoenergetic imaging from dual-source dual-energy computed tomography, Eur. J. Radiol. 122 (2020), 108666.
[46] F.G. Meinel, A. Graef, F. Bamberg, S.F. Thieme, F. Schwarz, W.H. Sommer, C. Neurohr, C. Kupatt, M.F. Reiser, T.R. Johnson, Effectiveness of automated quantification of pulmonary perfused blood volume using dual-energy CTPA for the severity assessment of acute pulmonary embolism, Invest. Radiol. 48 (8) (2013) 563–569.
[47] E.K. Weidman, A.J. Plodkowski, D.F. Halpenny, S.A. Hayes, R. Perez-Johnston, J. Zheng, C. Moskowitz, M.S. Ginsberg, Dual-energy CT angiography for detection of pulmonary emboli: incremental benefit of iodine maps, Radiology 289 (2) (2018) 546–553.
[48] W. Abdellatif, E. Esslinger, K. Kobes, A. Wong, J. Powell, I.T. Ali, G. Andrews, S. Nicolaou, Acquisition time, radiation dose, subjective and objective image quality of dual-source CT scanners in acute pulmonary embolism: a comparative study, Eur. Radiol. 30 (5) (2020) 2712–2721.
[49] L. Lenga, F. Trapp, M.H. Albrecht, J.L. Wichmann, A.A. Johnson, I. Yel, T. D'Angelo, C. Booz, T.J. Vogl, S.S. Martin, Single- and dual-energy CT pulmonary angiography using second- and third-generation dual-source CT systems: comparison of radiation dose and image quality, Eur. Radiol. 29 (9) (2019) 4603–4612.
[50] E.G. Kikano, M. Rajdev, K.Z. Salem, K. Laukamp, C.D. Felice, R.C. Gilkeson, A. Gupta, Utility of iodine density perfusion maps from dual-energy spectral detector CT in evaluating cardiothoracic conditions: a primer for the radiologist, AJR Am. J. Roentgenol. 214 (4) (2020) 775–785.
[51] T. D'Angelo, L. Lenga, C.T. Arendt, A.M. Bucher, J.L. Peterke, D. Caruso, S. Mazziotti, G. Ascenti, A. Blandino, A.E. Othman, S.S. Martin, M.H. Albrecht, B. Bodelle, T.J. Vogl, J.L. Wichmann, Carotid and cerebrovascular dual-energy computed tomography angiography: optimization of window settings for virtual monoenergetic imaging reconstruction, Eur. J. Radiol. 130 (2020), 109166.
[52] T. D'Angelo, G. Cicero, S. Mazziotti, G. Ascenti, M.H. Albrecht, S.S. Martin, A. E. Othman, T.J. Vogl, J.L. Wichmann, Dual energy computed tomography virtual monoenergetic imaging: technique and clinical applications, Br. J. Radiol. 92 (1098) (2019), 20180546.
[53] M. Okada, Y. Kunihiro, Y. Nakashima, T. Nomura, S. Kudomi, T. Yonezawa, K. Suga, N. Matsunaga, Added value of lung perfused blood volume images using dual-energy CT for assessment of acute pulmonary embolism, Eur. J. Radiol. 84 (1) (2015) 172–177.
[54] Y. Nagayama, T. Nakaura, S. Oda, D. Utsunomiya, Y. Funama, Y. Iyama, N. Taguchi, T. Namimoto, H. Yuki, M. Kidoh, K. Hirata, M. Nakagawa, Y. Yamashita, Dual-layer DECT for multiphasic hepatic CT with 50 percent iodine load: a matched-pair comparison with a 120 kVp protocol, Eur. Radiol. 28 (4) (2018) 1719–1730.
[55] M.H. Albrecht, C.N. De Cecco, U.J. Schoepf, A. Spandorfer, M. Eid, D. De Santis, A. Varga-Szemes, M. van Assen, P.L. von Knebel-Doeberitz, C. Tesche, V. O. Puntmann, E. Nagel, T.J. Vogl, J.W. Nance, Dual-energy CT of the heart current and future status, Eur. J. Radiol. 105 (2018) 110–118.
[56] R. Raju, A.G. Thompson, K. Lee, B. Precious, T.H. Yang, A. Berger, C. Taylor, B. Heilbron, G. Nguyen, J. Earls, J. Min, P. Carrascosa, D. Murphy, C. Hague, J. A. Leipsic, Reduced iodine load with CT coronary angiography using dual-energy imaging: a prospective randomized trial compared with standard coronary CT angiography, J. Cardiovasc. Comput. Tomogr. 8 (4) (2014) 282–288.
[57] V. Neuhaus, N. Grosse Hokamp, N. Abdullayev, R. Rau, A. Mpotsaris, D. Maintz, J. Borggrefe, Metal artifact reduction by dual-layer computed tomography using virtual monoenergetic images, Eur. J. Radiol. 93 (2017) 143–148.
[58] H. Yamauchi, M. Buehler, M.M. Goodsitt, N. Keshavarzi, A. Srinivasan, Dual-energy CT-based differentiation of benign posttreatment changes from primary or recurrent malignancy of the head and neck: comparison of spectral hounsfield units at 40 and 70 keV and iodine concentration, AJR Am. J. Roentgenol. 206 (3) (2016) 580–587.
[59] E.G. Odisio, M.T. Truong, C. Duran, P.M. de Groot, M.C. Godoy, Role of dual-energy computed tomography in thoracic oncology, Radiol. Clin. North Am. 56 (4) (2018) 535–548.
[60] A. Otrakji, S.R. Digumarthy, R. Lo Gullo, E.J. Flores, J.A. Shepard, M.K. Kalra, Dual-energy CT: spectrum of thoracic abnormalities, Radiographics 36 (1) (2016) 38–52.
[61] J. Izaaryene, V. Vidal, J.M. Bartoli, A. Loundou, J.Y. Gaubert, Role of dual-energy computed tomography in detecting early recurrences of lung tumours treated with radiofrequency ablation, Int. J. Hyperthermia 33 (6) (2017) 653–658.
[62] J.R. Wortman, P.M. Bunch, U.P. Fulwadhva, G.A. Bonci, A.D. Sodickson, Dual-energy CT of incidental findings in the abdomen: can we reduce the need for follow-up imaging? AJR Am. J. Roentgenol. 207 (4) (2016) W58–W68.
[63] D.I. Glazer, K.E. Maturen, R.K. Kaza, I.R. Francis, N.R. Keshavarzi, R.A. Parker, J. F. Platt, Adrenal Incidentaloma triage with single-source (fast-kilovoltage switch) dual-energy CT, AJR Am. J. Roentgenol. 203 (2) (2014) 329–335.
[64] N.G. Hokamp, A. Gupta, Evaluation of lung transplant perfusion using iodine maps from novel spectral detector computed tomography, Indian J. Radiol. Imaging 28 (4) (2018) 436–438.
[65] R. Rubinshtein, T.D. Miller, E.E. Williamson, J. Kirsch, R.J. Gibbons, A.N. Primak, C.H. McCollough, P.A. Araoz, Detection of myocardial infarction by dual-source coronary computed tomography angiography using quantitated myocardial scintigraphy as the reference standard, Heart 95 (17) (2009) 1419–1422.
[66] P.M. Carrascosa, A. Deviggiano, C. Capunay, R. Campisi, M. Lopez de Munain, J. Vallejos, C. Tajer, G.A. Rodriguez-Granillo, Incremental value of myocardial perfusion over coronary angiography by spectral computed tomography in patients with intermediate to high likelihood of coronary artery disease, Eur. J. Radiol. 84 (4) (2015) 637–642.
[67] M. Aoki, K. Hirose, M. Sato, H. Akimoto, H. Kawaguchi, Y. Hatayama, I. Fujioka, M. Tanaka, S. Ono, Y. Takai, Prognostic impact of average iodine density assessed by dual-energy spectral imaging for predicting lung tumor recurrence after stereotactic body radiotherapy, J. Radiat. Res. 57 (4) (2016) 381–386.

[68] L. Lenga, D. Leithner, J.L. Peterke, M.H. Albrecht, T. Gudauskas, T. D'Angelo, C. Booz, R. Hammerstingl, T.J. Vogl, S.S. Martin, J.L. Wichmann, Comparison of radiation dose and image quality of contrast-enhanced dual-source CT of the chest: single-versus dual-energy and second-versus third-generation technology, AJR Am. J. Roentgenol. 212 (4) (2019) 741–747.
[69] R.W. Bauer, S. Kramer, M. Renker, B. Schell, M.C. Larson, M. Beeres, T. Lehnert, V. Jacobi, T.J. Vogl, J.M. Kerl, Dose and image quality at CT pulmonary angiography-comparison of first and second generation dual-energy CT and 64-slice CT, Eur. Radiol. 21 (10) (2011) 2139–2147.
[70] A. Lapointe, H. Bahig, D. Blais, H. Bouchard, E. Filion, J.F. Carrier, S. Bedwani, Assessing lung function using contrast-enhanced dual-energy computed tomography for potential applications in radiation therapy, Med. Phys. 44 (10) (2017) 5260–5269.
[71] K. Ansari-Gilani, R.C. Gilkeson, E.G. Kikano, B.D. Hoit, Multimodality approach to the diagnosis and management of constrictive pericarditis, Echocardiography 37 (4) (2020) 632–636.
[72] E. Kikano, N. Grosse Hokamp, L. Ciancibello, N. Ramaiya, C. Kosmas, A. Gupta, Utility of virtual monoenergetic images from spectral detector computed tomography in improving image segmentation for purposes of 3D printing and modeling, 3D Print Med 5 (1) (2019) 1.
[73] B. Hochhegger, G.R. Alves, K.L. Irion, C.C. Fritscher, L.G. Fritscher, N.H. Concatto, E. Marchiori, PET/CT imaging in lung cancer: indications and findings, J. Bras. Pneumol. 41 (3) (2015) 264–274.
[74] T. Beyer, D.W. Townsend, T. Brun, P.E. Kinahan, M. Charron, R. Roddy, J. Jerin, J. Young, L. Byars, R. Nutt, A combined PET/CT scanner for clinical oncology, J. Nucl. Med. 41 (8) (2000) 1369–1379.
[75] C.N. De Cecco, P. Burchett, M. van Assen, J. Ravenel, S.L. Cooper, H. Li, M. L. Bradshaw, W.J. Rieter, U. Joseph Schoepf, L. Gordon, Rationale and design of a prospective study on the first integrated PET/dual-energy CT system for staging and image-based radiation therapy planning of lung cancer, Eur. Radiol. Exp. 2 (1) (2018) 15.
[76] G. Wang, PET-enabled dual-energy CT: a proof-of-concept simulation study, in: 2018 IEEE Nuclear Science Symposium and Medical Imaging Conference Proceedings (NSS/MIC), IEEE, 2018, pp. 1–4.
[77] M.J. Willemink, M. Persson, A. Pourmorteza, N.J. Pelc, D. Fleischmann, Photon-counting CT: technical principles and clinical prospects, Radiology 289 (2) (2018) 293–312.
[78] S. Leng, M. Bruesewitz, S. Tao, K. Rajendran, A.F. Halaweish, N.G. Campeau, J. G. Fletcher, C.H. McCollough, Photon-counting detector CT: system design and clinical applications of an emerging technology, Radiographics 39 (3) (2019) 729–743.
[79] A. Pourmorteza, R. Symons, V. Sandfort, M. Mallek, M.K. Fuld, G. Henderson, E. C. Jones, A.A. Malayeri, L.R. Folio, D.A. Bluemke, Abdominal imaging with contrast-enhanced photon-counting CT: first human experience, Radiology 279 (1) (2016) 239–245.
[80] R.J. Gillies, P.E. Kinahan, H. Hricak, Radiomics: images are more than pictures, they are data, Radiology 278 (2) (2016) 563–577.
[81] K. Bera, V. Velcheti, A. Madabhushi, Novel quantitative imaging for predicting response to therapy: techniques and clinical applications, Am. Soc. Clin. Oncol. Educ. Book 38 (38) (2018) 1008–1018.
[82] K. Bera, K.A. Schalper, D.L. Rimm, V. Velcheti, A. Madabhushi, Artificial intelligence in digital pathology - new tools for diagnosis and precision oncology, Nat. Rev. Clin. Oncol. 16 (11) (2019) 703–715.
[83] M. Seidler, B. Forghani, C. Reinhold, A. Perez-Lara, G. Romero-Sanchez, N. Muthukrishnan, J.L. Wichmann, G. Melki, E. Yu, R. Forghani, Dual-energy CT texture analysis with machine learning for the evaluation and characterization of cervical lymphadenopathy, Comput. Struct. Biotechnol. J. 17 (2019) 1009–1015.